The Graduate University for Advanced Studies, SOKENDAI

DOCTORAL THESIS

Beam polarization effects on Higgs boson production at the International Linear Collider

---

Author:
QUACH My Uyen Nhi

Supervisor:
Dr. Junpei FUJIMOTO

A thesis submitted in fulfillment of the requirements for the degree of Doctor of Philosophy

in the

Department of Particle and Nuclear Physics

School of High Energy Accelerator Science

December 10, 2020

The Graduate University for Advanced Studies, SOKENDAI

Abstract

Department of Particle and Nuclear Physics

Doctor of Philosophy

Beam polarization effects on Higgs boson production at the International Linear Collider

by QUACH My Uyen Nhi

The International Linear Collider (ILC) is a proposed international e^+e^- linear collider with beam energies ranging from 250 GeV to 1 TeV. ILC is supposed to start at the center-of-mass energy of 250 GeV in its initial stage to obtain high statistics measurements of the Higgs. Note that this center-of-mass energy was used for the calculations in this thesis.

Owing to parity violation in weak interactions, beam polarization effects are essential to resolve new phenomena beyond the Standard Model (BSM), and hence, studying these effects is necessary. Beam polarization and its importance in studying the physics at the e^+e^- collider have been discussed in detail over decades. A precise measurement to study the properties of the Higgs boson is one of the key targets of the ILC experiments. However, to achieve this, one needs to know the $\mathcal{O}(\alpha)$ corrections to the underlying processes.

In this thesis, I studied nine processes of $e^+e^- \to f\bar{f}H$ with the ILC polarized electron and positron beams of 250 GeV center-of-mass energy, which present the production of: (1) muon pair and Higgs boson, (2) electron-positron pair and Higgs boson, (3) tau pair and Higgs boson, (4) muon-neutrino pair and Higgs boson, (5) electron-neutrino pair and Higgs boson, (6) up-quark pair and Higgs boson, (7) down-quark pair and the Higgs boson, (8) charm-quark pair and Higgs boson, and finally (9) bottom-quark pair and the Higgs boson (note that I did not consider the production of top quark, strange quark, and tau-neutrino). I calculated the $\mathcal{O}(\alpha)$ corrections to each of these nine elementary particle reactions as well as the one-photon emission process using the on-shell renormalization scheme.

In this thesis, I used the GRACE-Loop system to calculate the amplitudes automatically. I developed two sets of Fortran codes. The first set was used to calculate the $O(\alpha)$ corrections corresponding to the one-loop diagrams and the one-photon emission processes; in this case, all the fermion masses were kept non-zero, except the neutrino mass, and the arbitrary longitudinal polarizations of the input electron and positron beams were available. The second set was used to treat the effects of initial-state radiation (ISR). The effects of one-loop weak corrections were determined by comparing the $O(\alpha)$ corrections with the ISR effects.

I verified the one-loop ampitudes generated by the GRACE-Loop system numerically by performing the following checks: (1) renormalization; (2) infrared (IR) finiteness by adding the one-loop amplitudes and soft-photon effects, while introducing a fictitious photon mass; (3) gauge-parameter independence of the one-loop amplitudes with a set of five non-linear gauge fixing parameters; (4) soft-photon energy cut independence between the one-loop and the hard-photon emission amplitudes; in this check, I needed to perform a phase-space integration of the one-loop amplitudes. The one-loop amplitudes of the full Lagrangian are very large; and hence, challenging to compute numerically.

Considering the above points, I introduced "NOLLS approximation", where the couplings between the light-fermions (except for the bottom- and top-quarks) and scalar particles are neglected, and the masses of all fermions are retained. I confirmed the one-loop amplitudes generated using the NOLLS approximation to be consistent with those obtained from the Monte-Carlo integration of the full Lagrangian. Therefore, in this thesis, I only present and discuss the results obtained using the NOLLS approximation.

In this work, I also present a comparison with the cross-sections of $H\nu\bar{\nu}$ obtained without beam polarization in previous work. The integration errors for all cases are presented. Moreover, I confirm the k_c independence for all the cases. The accuracy of my $\mathcal{O}(\alpha)$ calculations is approximately 0.2% for all the processes.

I also calculated the $\mathcal{O}(\alpha)$ corrections to nine processes $e^+e^- \to f\bar{f}H$ using the beam polarizations of the proposed ILC. The size of $\mathcal{O}(\alpha)$ corrections reached appoximately -10% for these polarized beams, i.e., in the absence of any experimental cut.

Originally the GRACE-Loop system can produce the codes of the polarized $\mathcal{O}(\alpha)$corrections, but there is no function to generate such common codes to treat arbitrary beam polarization then I added this part. It is my contribution to the GRACE-Loop system.

Note that the analysis of the recoil mass distribution is crucial, as it allows the analysis of the g_{HZZ} coupling without any assumptions of the branching ratio of the Higgs boson decay. The $\mathcal{O}(\alpha)$ corrections induce a significant change, especially by the initial state radiation, so-called the radiative tail. I calculated the recoil mass distribution after applying three kinds of experimental cuts on the $\mathcal{O}(\alpha)$ corrections to the process $e^+e^- \to \mu^+\mu^- H$ and by including the ISR effects. I obtained the following corrections $\delta_{Total} = -16.9\%$ and $\delta_{ISR} = -13.8\%$; thus the weak correction was estimated to be -3%. Therefore, if one wants to measure the g_{HZZ} coupling within an accuracy of 1%, a weak corrections of -3% cannot be neglected.

I also compared the channels of leptons and quarks. With leptons, δ_{ISR} for the s-channel and t-channel processes were approximately 10%, and 18%, respectively; whereas with quarks, $\delta_{ISR}(s)$ were approximately 10% for all cases, using the polarized beams of the ILC and without any experimental cuts. Comparing the channels of leptons and quarks, reveals the difference between the up-type and down-type quarks; however, it is not the case for the leptons.

In conclusion, my calculations have the following features: (1) the beam polarization effects were considered, (2) mass effects of all the fermions except neutrinos were retained, and (3) Yukawa coupling of the bottom quark

was included. To the best of my knowledge, this is the first detailed discussion of the $e^+e^- \to f\bar{f}H$ processes all over the world. Furthermore, I compared the cross-sections and the total ratios, which are obtained by electroweak $\mathcal{O}(\alpha)$ corrections and those of the ISR effects. This discussion is also performed for the first time ever, which is important for the analysis of experimental data.

Committee Members

The thesis of QUACH My Uyen Nhi was reviewed and approved by the following:

HASHIMOTO, Shoji
Professor of High Energy Accelerator Research Organization (KEK)
Professor of The Graduate University for Advanced Studies, SOKENDAI
Department of Particle and Nuclear Physics
Chief examiner

NOJIRI, Mihoko
Professor of High Energy Accelerator Research Organization (KEK)
Professor of The Graduate University for Advanced Studies, SOKENDAI
Department of Particle and Nuclear Physics

OMORI, Tsunehiko
Lecturer of High Energy Accelerator Research Organization (KEK)
Lecturer of The Graduate University for Advanced Studies, SOKENDAI
Department of Particle and Nuclear Physics

FUJIMOTO, Junpei
Lecturer of High Energy Accelerator Research Organization (KEK)
Lecturer of The Graduate University for Advanced Studies, SOKENDAI
Department of Particle and Nuclear Physics
Chief Supervisor

KURIHARA, Yoshimasa
Lecturer of High Energy Accelerator Research Organization (KEK)
Lecturer of The Graduate University for Advanced Studies, SOKENDAI
Department of Particle and Nuclear Physics
Vice Supervisor

FUJII, Keisuke
Senior Fellow, Emeritus Professor of High Energy Accelerator Research Organization (KEK)
Department of Particle and Nuclear Physics
External review committee

Acknowledgements

Before starting this doctoral thesis, I would like to express my gratitude and my apologies to important people in my life. I did not expect a PhD journey of having such obstacles. I made countless mistakes. Thank you so much for your kindness, patience and forgiveness. This thesis would not have been possible without their intellectual and emotional support.

First of all, I am forever grateful to my supervisor, Prof. Junpei Fujimoto who accepted me as his student for my last 2 years of my PhD period. Without him, I could not have finished my PhD. I appreciate his taking many long hours of teaching and giving me valuable advice. His patience and continuous encouragement helped me to build up my confidence to pursue my PhD through the most difficult period. He kept guiding and encouraged me that my thesis was extremely important for high energy physics especially for the ILC project which made me feel more responsible and more meaningful. He was a great role-model of overcoming difficulties for me to follow. According to Japanese Zen Buddhist Philosophy, one should try to show the best performance regardless of the circumstances, which I learned from him was highly motivated. He was also extremely supportive and kind to me. The phrase he said "mou chotto" (just a little more) which I receive from him every single day gave me belief that I could complete my PhD.

Secondly, I am deeply indebted to my vice-supervisor, Prof. Yoshimasa Kurihara for his guidance, support and encouragement throughout my studies. I am extremely grateful for his giving me the opportunity to study in Japan, letting me join the GRACE group and teaching me how to do research with physics and programming knowledge. His teaching method was tremendously powerful and encouraging. I enjoyed the privilege of being his student. He has been a great influence on my research life. His honesty and work ethic inspired me immensely. He has always been a brilliant and inspiring physicist whom I respect and admire particulaly. He also gave me the chances to attend various international schools and conferences which were some of the best moments during my PhD time. I am sincerely appreciative of his giving me plentiful help before and during my PhD thesis defense. He was a great supervisor with his extremely patience, extraordinary generosity, and constant support not only in academics but also in daily life. I am beyond grateful for his significant effort during my mentally unstable period. Moreover, his willingness to help me on solving problems and his warmness made him become the closest person to me in Japan especially throughout my early years of graduate school.

I would like to express my sincere appreciation to the PhD defense committee members giving me a lot of fruitful questions, comments and encouragement:

I thank Prof. Shoji Hashimoto for agreeing to chair my doctoral thesis committee and asking me a lot of questions as well as giving me many suggestions.
I thank Prof. Keisuke Fujii for pointing out the unique parts of my thesis defense and reviewing my thesis extra detailedly and carefully.
I thank Prof. Mihoko Nojiri for requesting me to improve theory parts in my thesis.
I thank Prof. Tsunehiko Omori for helpful information on my thesis defense.
I thank Prof. Yoshimasa Kurihara for his support and encouragement during the thesis defense.
Thank you very very much!

I also would like to thank Professors at KEK/SOKENDAI who gave me many helpful lectures and were willing to answer my questions.

I would like to thank Prof. Hioki Zenro for providing me the file MW1.f to calculate m_W and Δr. I would like to send my thanks to members of GRACE group: Prof. Fukuko Yuasa, Prof. Toshiaki Kaneko for their numerous discussions and extremely careful, detail comments. Additionally, I also would like to extra thank Prof. Fukuko Yuasa because of her gentle, sophisticated care.

Thanks SOKENDAI staff worked hard on preparing for my documents. Thanks Prof.Shoji Hashimoto and Prof. Mihoko Nojiri for spending time for me every few months even they are extremely busy with various duties.

Finance was a very challenging issue to me. Heiwa Nakajima and Inner Trip Foundation have been supporting me during my PhD period. The RA job offered by KEK, and SOKENDAI tuition fee reduction and exemption were very helpful. I also would like to thank Mc Donald restaurant where offered me the first part time job. Thanks KEK Daily Yamazaki convenient store owners for always being kind and friendly to me.

Thanks Japanese and Vietnamese doctors who gave me the proper treatment on my disease.

Some friends in Japan who were nice to me especially Prof. Etienne Forest. I am grateful for Prof. Shoji Uno who was kindly took me to many beautiful landscapes and historical monuments of Japan.

I cannot forget to thank my undergraduate supervisor, Prof. Pham Quang Hung for his encouragement and positive thoughts.

I would like to thanks Tikubi and friends. Tikubi came at the most difficult moment of my life to gradually recover my confidence and convinced me that I was not a useless person. Thanks to Tikubi, I had very good Vietnamese friends, who gave me fun time especially Huyen Nguyen was a very

supportive friend. She helped me to work on many important documents.

I would like to send special thanks to my foster father, Prof. Tokio Ohska who always cared and helped me unconditionally whenever I needed him. He gave me valuable lessons not only in Japanese but also in life. At my graduate student days, he was the person who had the most influence on improving my cognition and positive attitude. I cannot dare to imagine how my life in Japan would have been without him especially during my most challenging period. He gave me the chances to make mistakes and corrected them to become a more mature person. He was always with me regardless of the thousand mistakes I made without blaming. He treated me as his "princess" as well as a little daughter. He has been pampering me constantly but never hesitated to point out my improper actions or behaviors. I learned through him as great role-model but not criticizing. He is an extremely wise, generous, and sophisticated person. He is definitely my lucky charm.

I am deeply indebted to my parents for their unconditional love and care. Words can never be enough in expressing my thanks to them for their encouragements, help, and warmness. I also would like to thank my younger brother, Tai Quach for helping me many things. My special thank is for my little sister, Anh Quach. She was also my best female friend. I could just tell her everything happened in my life every single day. She was definitely my muse.

Thanks my husband, Dr. Constantino Calancha Paredes for his sacrifice to help me focus on finishing this PhD thesis. He taught me not only to stand up for myself and fight for what I believe, but also to slow down and enjoy life. I could never ask for a better life partner. Long-term and long-distance relationship was particularly challenging, I am profoundly appreciative of his effort. He was my great motivation to keep working on my PhD.

In the end, I have realized Japan and people here were kind to me. The writing of this thesis has been a very long journey with many ups and downs. The process made me more humble and grateful for what I have and the people I met along the way.

To everyone who knows about my thesis and has me in your concern, THANK YOU!

Dedication

This thesis is dedicated to the 40th birthday of my husband, Constantino Calancha Paredes. Without his love and encouragement, I would never have been able to complete my graduate study.

This thesis is also dedicated to my parents and my foster father. I love you all and I appreciate everything that you have done for me.

Contents

List of Figures

List of Tables

Chapter 1

The Standard Model

1.1 Brief introduction to the Standard Model

One of the main objectives of modern physics is to find the answer to the question: What is the universe made of?. However, the answer is still elusive. The universe is composed of dark energy, dark matter, and ordinary matter. According to the current data, dark energy dominates and makes up approximately 68.3% of the universe, followed by dark matter and ordinary matter, which make up 26.8% and 4.9% of of the universe, respectively [4]. Fig. 1.1 shows the composition of the universe.

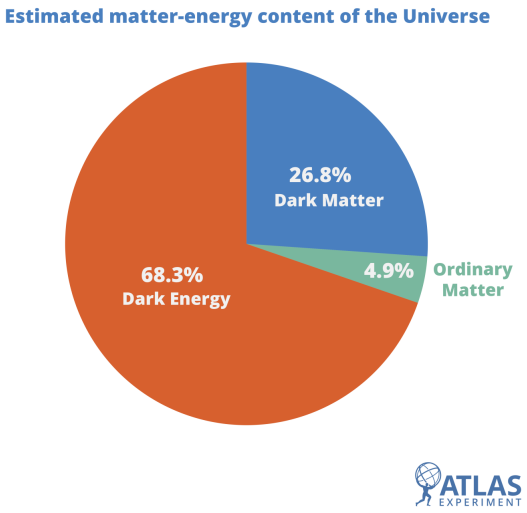

FIGURE 1.1: Percentage of ordinary matter, dark matter, and dark energy in the universe, as measured by the Planck satellite[1].

Ordinary matter in the universe is composed of particles that can be described by the field of particle physics. An elementary particle is a particle without any determinable substructure; however, it is not known whether such a particle is composed of other particles. Known elementary particles include the fundamental fermions (i.e., quarks, anti-quarks, leptons, and anti-leptons), which are the matter or anti-matter particles, and the vector

bosons (i.e., gauge bosons), which are the "force particles" that mediate interactions among particles. The Higgs boson, after its recent discovery, has been added to this list. The Higgs field is responsible for the spontaneous symmetry breaking of the electroweak symmetry, and, it consequently gives particles in the Standard Model (SM), namely, quarks, leptons, the W and Z gauge bosons, and their masses. There are six types of quarks: known as up (u), down (d), charm (c), strange (s), bottom (b), and top (t). Each of these quarks also has a corresponding anti-particle. There are also six types of leptons: electron (e), muon (μ), tau (τ) and their corresponding neutrinos, ν_e, ν_μ, ν_τ. These quarks and leptons are paired into three left-handed doublets and six right-handed singlets. Conversely, right-handed particles can only form singlets. These doublets and singlets constitue three generations of the quarks and leptons. Fig. 1.2 illustrates the particles of the SM.

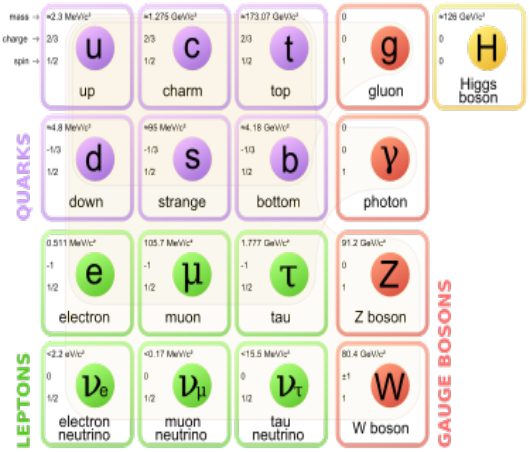

FIGURE 1.2: The SM of elementary particles.

There are four types of interactions among elementary particles: electromagnetic, weak, strong, and gravitational. The gravitational interactions are much weaker than the strong, weak, and electromagnetic interactions and hence are usually neglected. The fundamental interactions among elementary particles are described using gauge theories, as demonstrated by Fig. 1.3. The gauge theory describing the weak and electromagnetic interactions among quarks and leptons is represented by the gauge group $SU(2)_L \otimes U(1)_Y$, which spontaneously breaks to give rise to the electromagnetic gauge group $U(1)_{em}$, consequently, the massive W and Z bosons and a massless photon. The strong interactions among quarks are described by the color gauge group $SU(3)_c$, consiting of eight gluons. The gauge group describing the strong, weak, and electromagnetic interactions of quarks and leptons represented by $SU(3)_c \otimes SU(2)_L \otimes U(1)_Y$. These interactions are consistent with the experimental data obtained at various accelerators at both low and high energies.

A very important aspect of the SM is the presence of the Higgs field, whose non-vanishing vacuum expectation value spontaneously breaks the

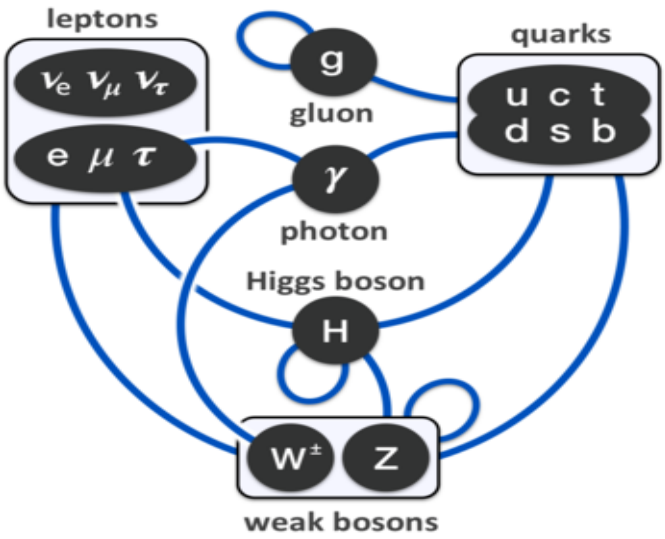

FIGURE 1.3: Summary of interactions between particles described by the SM. The blue lines represent interactions of the gauge bosons and the Higgs boson with quarks and leptons.

electroweak symmetry of $SU(2)_L \otimes U(1)_Y$ to $U(1)_{em}$. During this process, the weak gauge bosons $W^{\pm}$ and Z as well as the quarks and leptons, obtain masses. This is commonly referred to as the Brout-Englert-Higgs mechanism. On July 4, 2012, the discovery of a new particle with properties similar to the Higgs boson was announced, which led to a Nobel Prize in physics for Peter Higgs and Francois Englert. After more data were analyzed, physicists confirmed that the Higgs boson indeed exists. The Higgs boson is the first fundamental scalar particle discovered in nature and is the key to affirming the existence of the Higgs field.

The top quark is the heaviest particle in the SM, and it couples strongly to the Higgs field. Moreover, the masses of the Higgs boson and top quark affect the vacuum stability of the SM. Therefore, the precise measurement of these particles is crucial, and is one of the major goals of physicists to understand the laws of nature.

Although the SM is very successful in describing the known fundamental interactions, it cannot answer several basic questions such as: Why are there three generations of quarks and leptons? What are the features of quark (as well as lepton) mass hierarchy and mixing? What is the nature of dark matter?

To answer some of the aforementioned questions, one needs to explore theories beyond the Standard Model (BSM). More importantly, to search for signals from BSM, one needs to know the precise measurements of particles in the SM. The International Linear Collider (ILC), which is a complementary

accelerator to the Large Hadron Collider (LHC), may pave the way to solve some of these mysteries.

Chapter 2

The International Linear Collider

2.1 Introduction

The ILC is a future linear electron-positron collider, operating at 250 to 500 GeV center-of-mass energies with high luminosity which can be extended to 1 TeV in the upgrade stage. It is, based on 1.3 GHz superconducting radio-frequency (SCRF) accelerating technology [5]. The ILC is proposed to be constructed in the Kitakami Mountains inTohoku area, Japan. It is an international project running for more than 20 years collaborated by more than 300 institutes, universities, and laboratories.

The major physics aim of the ILC is to determine the future direction of particle physics via precise measurements of the couplings of the Higgs boson with other elementary particles. A wide variety of elementary particle and nuclear physics can be studied. ILC accelerator consists of electron gun, positron generator, two 5 GeV injectors, two 5 GeV damping rings, transport lines to the far end of Linacs, and two 125 GeV superconducting linear accelerators, two final focus beam lines and two beam dumps.

The ILC parameters have been chosen by the particle physics community based on the requirements from 2003 to date. The ILC design is the result of over twenty years of R&D. The superconducting cavities, which are the most essential parts of the ILC, are based on decades of groundbreaking research by the TESLA technology collaboration in the 1990s.

2.2 Physics targets of the ILC

On July 4, 2012, the Higgs boson discovery was announced by physicists in two experiments (CMS and ATLAS) of the LHC at CERN. A new subatomic particle with a mass of approximately 125 GeV and several other properties of the Higgs boson, as predicted by the SM, were observed [6],[7]. The Higgs boson discovery made the SM of particle physics complete.

The prediction of additional Higgs bosons is one of the prominent features of possible physics BSM, which leads to an extended Higgs-boson sector. Searching for higher-mass Higgs bosons is also very interesting to physicists. However, the hypothesis that the Higgs boson is heavy and approaches

the theoretical upper bound has been validated by the expected exclusion regions with 300 fb^{-1} and 3 ab^{-1} LHC data, if no BSM is present. Therefore, the ILC is an exemplary collider to study the Higgs boson particle at 125 GeV. Irrespective of whether this newly discovered particle is one of the various possible Higgs boson or a completely different boson that mainly contributes to the masses of the Z and W bosons, it will be observed at the ILC.

If this new particle is one of various Higgs bosons and a different boson is the one that mainly contributes to the Z-boson and W-boson masses, that particle will also be observed at the ILC.

The ILC thus points to a bright future for the study of the Higgs field and its implications for high energy physics.
With 125 GeV Higgs particle, the first course at the ILC would be at threshold around $\sqrt{s} = 250$ GeV, which displays the clear peak cross section for the process $e^+e^- \to ZH$. At that energy, the precise measurements of Higgs recoil mass for the Higgs-strahlung process $e^+e^- \to ZH$ with subsequent $Z \to l^+l^-(l = e, \mu)$ decay is the most important measurement. This measurement allows a model-independent absolute measurement of the g_{HZZ} coupling. In this setting, measuring the proportion for all of Higgs boson decays including common final states or invisible decays with great accuracy is possible.
It is not necessary to observe the Higgs decay because corresponding hidden decay is observable. Nevertheless, the $e^+e^- \to ZH$ process can be used to measure diverse branching ratios for various Higgs decay processes. I included the $Z \to q\bar{q}$ and $Z \to \nu\bar{\nu}$ processes in my analysis to increase the statistical accuracy. The Higgs boson can also decay into a pair of W-bosons. However, the measurement of the WW-fusion process at $\sqrt{s} = 250$ GeV is quite difficult. Conversely, the W-pair production process becomes active at $\sqrt{s} = 500$ GeV, and hence the energy setting of the ILC needs to be changed accordingly, [7].

At $\sqrt{s} = 500$ GeV, the W-pair production process $e^+e^- \to \nu\bar{\nu}H$ dominates over the Higgs-strahlung process $e^+e^- \to ZH$. For the $\sigma \times BR$ measurements, this WW-fusion process is needed.
To make accurate measurements of the Higgs boson coupling to top quarks, the energy must be increased further. The top-Yukawa coupling measurements using the $e^+e^- \to t\bar{t}h$ process is probably even more exciting than the measurements of the branching ratio because it is the largest coupling among all the matter fermions.
The Higgs self-coupling measurement is another interesting study because we would like to detect the force that constructs the Higgs boson condense in the vacuum for the purpose of uncovering the electroweak symmetry breaking secret.

At higher energies, the WW-fusion processes become increasingly important. Note that the collider luminosity scales with the center-of-mass energy.

Thus, combining these factors together with the higher sensitivity of the ILC permits us to make a considerably better measurement of the Higgs self-coupling using the $e^+e^- \to \nu\bar{\nu}HH$ process with $\sqrt{s} = 1000$ GeV.
At $\sqrt{s} = 1000$ GeV, the top quark production process $e^+e^- \to t\bar{t}h$ is also near its maximal cross section, thus making the simultaneous measurements of the top-Yukawa coupling and the Higgs self-coupling feasible.

The ILC will also contribute to BSM by searching for new particles associated with dark matter, the Higgs field and other unsolved problems in particle physics. The LHC collider has limitations on detecting such electroweakly-interacting particles, which are associated with a large background and strong interaction induced processes. ILC experiments will either confirm or eliminate these particles based on the beam energies at each stage.

In conclusion, the ILC experiments will reveal unseen interactions by observing the pair-production of top quarks, Z and W bosons at higher energy. The precise measurement of Z boson's characteristics in a e^+e^- collider will also enhance our knowledge on the SM. This collider will improve the level of accuracy to the top quark and W-boson properties. The mass of the top quark will be measured at the ILC in a theoretically clean way that is impossible at LHC, fixing an important input to high energy physics calculations. The mass of top quark is the highest among particles of the SM, thus must have especially characteristic such as strong coupling to the Higgs field. The precise measurement of the top quark electroweak couplings might show some composite structure in the Higgs boson.
Note that one expects to observe characteristic effects of strong interactions in the Higgs field models, as well as in other models, where asymmetrical interactions associated with the Higgs fields are signs of hidden, extra space dimensions.

2.3 Design of the ILC

Fig. 2.1 shows a general view of the collider indicating the locations of the major sub-systems which are:

- A photocathode DC gun that creates a polarized electron beam.
- The electron main linac beam that passes through a long helical undulator to generate a multi-MeV photon beam and then bumps onto a thin metal target to generate longitudinally polarized positrons in electromagnetic showers. The ILC positron source generates the positron beam.
- Two 5 GeV electron and positron damping rings (DR);
- Two 5 GeV injectors.
- Two 125 GeV superconducting linear accelerators.

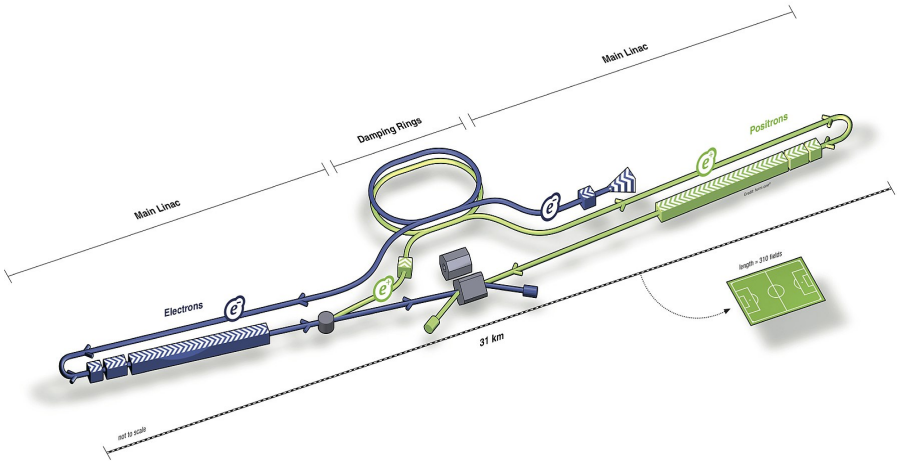

FIGURE 2.1: Schematic layout of the ILC, indicating all the major subsystems [2].

- Transport lines to the far end of the linacs.
- Two final focus beam lines.
- Two beam dumps.

2.4 Analysis of the ILC experiments

2.4.1 Beam polarization effects

Definitions and realistic polarization effects

The left-handed polarization degree of the electron beam is defined as,

$$p_e = (N_{e_R} - N_{e_L})/(N_{e_L} + N_{e_R}), \tag{2.1}$$

where N_{e_R} and N_{e_L} are the number of the right-handed and left-handed electrons in the beam, respectively [8],
and

$$p_p = (N_{p_R} - N_{p_L})/(N_{p_R} + N_{p_L}), \tag{2.2}$$

N_{p_R} and N_{p_L} are the number of the right-handed and left-handed positrons in the beam, respectively.
When a normalization $N_L + N_R = 1$ is used, the normalized number of left-handed and right-handed electrons can be obtained as $N_L = \frac{1-p_e}{2}$ and $N_R = \frac{1+p_e}{2}$, respectively.

Therefore, the cross-sections for a given combination of the electron and positron beam polarizations can be written as:

$$\sigma(p_e, p_p) = \frac{1}{4}\{(1-p_e)(1+p_p)\sigma_{LR} + (1+p_e)(1-p_p)\sigma_{RL} \\ +(1-p_e)(1-p_p)\sigma_{LL} + (1+p_e)(1+p_p)\sigma_{RR}$$

where σ_{LR} stands, for the cross-section with the 100 % left-handed polarized electron ($p_e = -1$) and the 100 % right-handed polarized positron ($p_p = +1$) beams. The cross-sections σ_{RL}, σ_{LL} and σ_{RR} are defined analogously.
Because of ignoring negligibly small (oder of 10^{-11}) cross-sections of σ_{LL} and σ_{RR} thus we have

$$\sigma(p_e, p_p) = \frac{(1-p_e)(1+p_p)}{4}\sigma_{LR} + \frac{(1+p_e)(1-p_p)}{4}\sigma_{RL} \tag{2.3}$$

The cross-sections with ILC proposed polarizations of the design value

$$p_e = \frac{0.1 - 0.9}{1} = -0.8 \tag{2.4}$$

and

$$p_p = \frac{0.65 - 0.35}{1} = 0.3 \tag{2.5}$$

can be obtained from those with 100% polarized results (p_e,p_p).

- $p_e = 0$, $p_p = 0$ UP: unpolarized
- $p_e = +1$, $p_p = +1$ RR: right-right polarization
- $p_e = -1$, $p_p = -1$ LL: left-left polarization
- $p_e = +1$, $p_p = -1$ RL: right-left polarization
- $p_e = -1$, $p_p = +1$ LR: left-right polarization
- $p_e = -0.8$, $p_p = 0.3$ ILC: ILC proposed polarization

where UP, RR, LL, RL, LR, and ILC stand for unpolarized; right-handed positron right-handed electron with full polarization; left-handed positron left-handed electron with full polarization; right-handed positron left-handed electron with full polarization; left-handed positron right-handed electron with full polarization; and with ILC proposed polarization $+30\%$ for e^+_R and -80% for e^-_L, respectively.

2.4.2 Recoil mass analysis

I introduce the recoil mass analysis that I conducted to make a model-independent measurement of the coupling between the Higgs and Z bosons, (i.e., g_{HZZ} coupling), using the recoil mass distribution in $e^+e^- \to ZH$ with

$Z \to \mu\mu$ [4].

In electron-positron collisions at $\sqrt{s}$ =250 GeV, the main Higgs production mechanism is the Higgs-strahlung process $e^+e^- \to HZ$. For $m_H = 125$ GeV, the cross section for the s-channel process is maximal close to $\sqrt{s} =$ 250GeV.
The total HZ cross section is proportional to the square of the coupling between Higgs and Z bosons, that is, $\sigma(e^+e^- \to HZ) \propto g^2_{HZZ}$, and the cross-sections of the decays to the final state in $H \to X\bar{X}$ can be expressed as

$$\sigma(e^+e^- \to HZ) \times BR(H \to X\bar{X}) \propto \frac{g^2_{HZZ} \times g^2_{HXX}}{\Gamma_H} \tag{2.6}$$

In this study, the cross-section of $e^+e^- \to HZ$ was measured using the recoil mass technique. I considerd $\sigma(e^+e^- \to HZ)$, and the recoil mass can be expressed as

$$m^2_{rec} = s - 2\sqrt{s}(E_{\mu^+} + E_{\mu^-}) + m^2_{\mu^+\mu^-},$$

where $\sqrt{s}$ is the center-of-mass energy, and $E_{\mu+}$ and $E_{\mu-}$ are the energies of the two muons and $m^2_{\mu^+\mu^-}$ is the invariant mass of muon and anti-muon from Z decay.

At $\sqrt{s} = 250$ GeV, where the energy of the muons from Z decay approximately scales as $\sqrt{s}$, the width of recoil mass distribution increases significantly with increasing center-of-mass energy. Therefore, the leptonic (in particular, muonic) recoil mass analysis leads to a higher precision on g_{HZZ} for $\sqrt{s} = 250$ GeV, where $\sigma(HZ)$ is the largest and the recoil mass peak is relatively narrow.
Using this technique, one can determine the absolute branching ratios of Higgs boson decays, including those of the invisible decays.

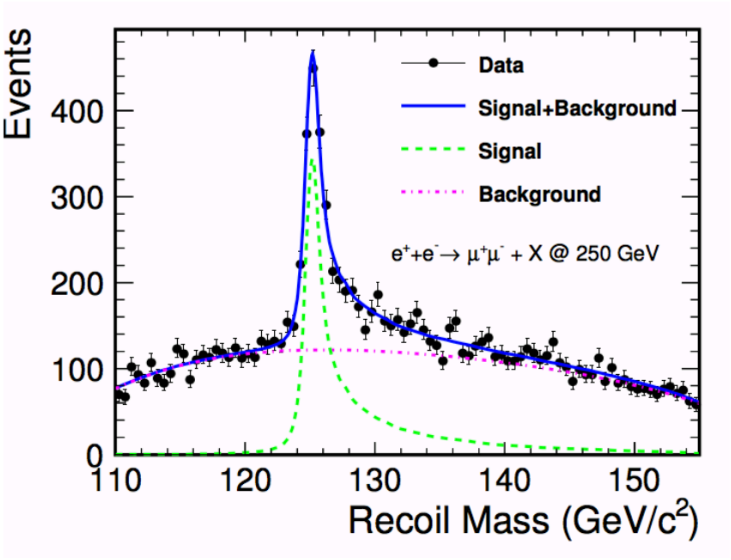

FIGURE 2.2: Recoil mass distribution of the Higgs-strahlung process $e^+e^- \to \mu^+\mu^- H$ ($e^+e^- \to ZH$ followed by $Z \to \mu^+\mu^-$) with 250 fb^{-1} for m_h = 120 GeV at $\sqrt{s} = 250$ GeV [3].

It should be noted that in this recoil mass distribution, the simple ISR and the detector resolution effects are included, which leads to the apperance of the tail structure in Fig. 2.2.

Chapter 3

Calculation methods

3.1 The GRACE-Loop system

In this section, I discuss the GRACE-Loop system [9]. First, I explain the necessity of automatic calculation. It is the motivation for GRACE to be created. Secondly, we introduce what GRACE is and its structure. Next, I confirm that GRACE satisfies the renormalization condition and performs the required system check. Finally, the beam polarization included in GRACE is described.

3.1.1 Motivation for automatic calculation

Collecting and analyzing data from high-energy experiments at large accelerators, such as LHC and ILC, are very complicated and tedious tasks. There are many steps that physicists need to do carefully and precisely. Briefly, the data are obtained from the collisions of beams then we analyze them by using some methods to reduce the background and gain the signal. Based on pertubation theory, theoretical calculation must treat both of the background and the signal exactly. The cross-sections (decay widths) which corresponds to events are simulated. In the end, one obtains the real events which fit to the collected data with the acceptable errors. From this, the precise theoretical calculation is one of the essential steps. With the traditional method (hand calculating), it is almost impossible to calculate the complicated processes. Thanks to the improvement of science and technology, numerical calculation method has become popular and contribute to high energy physics.

3.1.2 Introduction to the GRACE-Loop system

Definition

The GRACE-Loop system is a programming system for calculating at the tree level and full one-loop electroweak cross-sections automatically with beam-polarization based on the SM and the MSSM (Minimal Supersymmetric Standard Model) at high energy physics. This program was created and has been developed by MINAMI-TATEYA group at High Energy Accelerator Research Organization (KEK) [10]. The GRACE-Loop system primarily

focuses on evaluating one loop correction to the SM processes at electron-positron collision. Besides that, with the GRACE-Loop system, one can calculate one-loop corrections to the MSSM [11].

Structure

The structure of the GRACE-Loop system is quite complicated, as demonstrated by Fig. 3.1. The GRACE-Loop system uses the symbolic manipulation

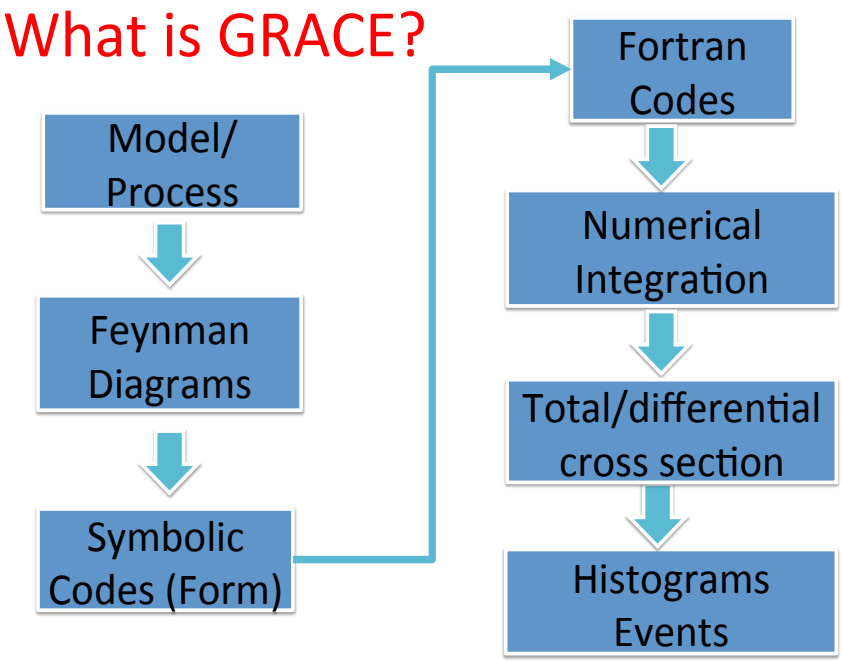

FIGURE 3.1: GRACE structure

system FORM [12] to calculate all Dirac and tensor algebra in n dimensions.

3.2 Renormalization and system check

In the GRACE-Loop system, renormalization is carried out with the on-shell condition in the Kyoto scheme [13]. The non-linear gauge fixing Lagrangian condition [14] is written as follows:

$$\mathcal{L}_{GF} = -\frac{1}{\xi_W} \mid (\partial_\mu - ie\tilde{\alpha}A_\mu - igc_W\tilde{\beta}Z_\mu)W^{\mu+} + \xi_W\frac{g}{2}(v+\tilde{\delta}H+i\tilde{\kappa}\chi_3)\chi^+ \mid^2$$
$$-\frac{1}{2\xi_Z}(\partial.Z+\xi_Z\frac{g}{2c_W}(v+\tilde{\epsilon}H)\chi_3)^2 - \frac{1}{2\xi_A}(\partial.A)^2.$$

To satisfy this condition, the results must be independent of the non-linear gauge parameters $\tilde{\alpha}, \tilde{\beta}, \tilde{\delta}, \tilde{\kappa}$, and $\tilde{\epsilon}$. Thus, various checks are required to confirm the precision of the system. The total cross-sections are given by

$$\sigma_{\mathcal{O}\alpha=\sigma_{Tree}+\sigma_{Loop}(C_{UV},\lambda,\tilde{\alpha},\tilde{\beta},\tilde{\delta},\tilde{\epsilon},\tilde{\kappa})+\sigma_{Tree}\delta_{soft}(\lambda,E_\gamma<k_c)+\sigma_{Hard}(k_c)} \tag{3.1}$$

where k_c is the parameter used to define the soft photon ($E_\gamma < k_c$) and hard photon ($E_\gamma \geq k_c$) energy cutt-off. By performing numerical checks using the GRACE-Loop system, I confirmed the following: ultraviolet coefficient (C_{UV}) independence, photon mass (λ) independence, gauge invariance ($\tilde{\alpha}, \tilde{\beta}, \tilde{\delta}, \tilde{\kappa}, \tilde{\epsilon}$) and k_c independence. The fictitious photon mass (λ) is added as a general treatment to regulate the infrared divergence. The reason why we choose the non-linear gauge parameters in our GRACE-Loop system instead of using the linear-gauge parameters: the non-linear gauge parameters only appear in the numerator, thus we can use the same Loop library to calculate while the linear-gauge parameters also appear in the denomerator . It is much more simple and avoids having unnecessary problems when we use non-linear gauge parameters.

3.2.1 One-loop renormalization

Renormalization scheme

Based on the experimental data, I determined a set of independent parameters to make the theoretical predictions. Renormalization theory yields the relations between the parameters and fields. Renormalization theory is very important because it provides a systematic way in which to deal with the divergences. A renormalization scheme is a way to pick for all interaction Lagrangians in these affine spaces, making them finite dimensional vector spaces relative to this specific choice. If the measured quantity can be evaluated exactly through considering all order of perturbation theory, it must be renormalization scheme independent. Nonetheless, the calculated observables depends on the different choices of schemes in the truncated perturbation theory, which is so-called scheme dependence. I chose the on-shell renormalization Kyoto scheme [13]. Since for most calculations in QED (as well as for many calculations in the theory of electroweak interactions), this is the most convenient renormalization scheme for my thesis. More detail on the electroweak on-shell renormalization scheme is presented at the Appendix B.

In this scheme, the renormalized mass and coupling constant are related to well-measured physical constants (e.g., the mass of the electron and the fine-structure constant α), and in which the renormalized fields are defined such that the propagator poles are located at the physical mass and the pole residues in the propagator remain equal to unity.

In the on-shell renormalization scheme, the input parameter set is chosen as $\{\alpha, m_W, m_Z,$ and Higgs mass as well as fermion masses $\}$ [8]. The Z boson mass has been precisely measured to be $m_Z = 91.1876 \pm 0.0021$ GeV as reported in [15]. This uncertainty is enough to probe the new physics signals at the future colliders. The W boson mass $m_W = 80.379 \pm 0.012$ GeV and the physical mass of the top quark $m_t = 172.9 \pm 0.4$ GeV are reported in [2]. The most updated precision at the LHC experiments, $\delta m_W = 12$ MeV is small enough to clarify the observational data. With highly accurate program at

the prospective colliders, the uncertainty of δm_W approximates to 4 MeV is expectable. For the purpose of reducing theoretical uncertainties, the m_W will be calculated as a function of m_Z, m_H and G_μ as following

$$m_W^2 = m_Z^2 \left\{ \frac{1}{2} + \sqrt{\frac{1}{4} - \frac{\pi\alpha}{\sqrt{2} G_\mu m_Z^2} [1 + \Delta r(m_W, m_Z, m_H, m_t, ...)]} \right\}, \tag{3.2}$$

where Δr summarizes radiative corrections to the muon decay width. Because Δr is dependent on the W-boson mass, the calculation of m_W is performed through iterative procedure from Eq.(3.1).

At the loop corrections, Δr is related to the large contributions of the mass of top quark.

Table 3.1 shows numerical values of m_W and Δr with the higher order corrections by means of MW1.f based on [16] provided by Prof. Z. Hioki as a function of of m_H, m_Z = 91.1876 GeV, m_t = 172.9 GeV and all other fermion masses.

m_H [GeV]	Δr	m_W [GeV]
125.1	0.02636986	80.3625

TABLE 3.1: The result for m_W is calculated by a Fortran program MW1.f with m_u = 58 MeV, m_d= 58 MeV, m_s= 92 MeV m_c= 1.5 GeV and m_b= 4.7 GeV as the same as Appendix A.

After chosing the input parameters, the total cross-section, $\sigma_{\mathcal{O}(\alpha)}$ is calculated at one-loop radiative corrections, the electroweak corrections can be read in this on-shell scheme as

$$\delta_{Total} = \frac{\sigma_{\mathcal{O}_\alpha}}{\sigma_{Tree}} - 1, \tag{3.3}$$

where σ_{Tree} is the cross-sections at the tree level. Because α is the input at Thomson limit, the δ_{Total} is called the electroweak correction in α-scheme. Consequently, δ_{Total} will be affected by a large contribution from the two-point function with the exchange of light-fermions. This contribution is of the form $log(s/m_f^2)$ with energy scale s and the light-fermion masses m_f .

3.2.2 Input parameters

For the calculation of the nine processes: ($\mu^+\mu^- H$, $e^+e^- H$, $\tau^+\tau^- H$, $\nu_\mu\bar{\nu}_\mu H$, $\nu_e\bar{\nu}_e H$, $u\bar{u}H$, $d\bar{d}H$, $c\bar{c}H$, and $b\bar{b}H$) at the ILC, we use the following input parameters. The masses of five types of quarks were chosen as: up quark mass 58.0×10^{-3} GeV, down quark mass 58.0×10^{-3} GeV, charm quark mass 1.5 GeV, strange quark mass 92.0×10^{-3} GeV, and the bottom quark mass 4.7 GeV. The reason I chose a set of light quark masses, is because these yields a "perturbative" value of m_W that is compatible with the current experimentally observed W-boson mass. I also set the masses of the top quark: 172.9

GeV. We use the mass of Z boson is 91.1876 GeV and the value of W mass of 80.379 GeV. We input Higgs boson mass of 125.1 GeV. Thomson limit is given by the fine structure constant alpha of 1/137.0359895. The Weinberg angle or weak mixing angle can be defined as $\sin^2\theta_W = 1 - \frac{m_W^2}{m_Z^2}$. A summary of the input parameters is provided in the Appendix A.

3.2.3 Polarization

In the GRACE-Loop system, at the tree level, polarization is taken into account from beginning with helicity amplitude method: using numerical calculation. Nevertheless, at the full one-loop electroweak correction, it is much more complicated hence the trace method by summing the square of the amplitude is used then to include polarization effect, we multiply the projection operators $\frac{1\pm\gamma_5}{2}$ into amplitude. It makes program size become much larger.

3.3 Radiator method

The effect of the initial photon emission can be factorized when the total energy of the emitted photons is sufficiently small compared to the beam energy or for small angle (co-linear) emissions.This approximation is referred as to the "soft-colinear photon approximation(SPA)". Under SPA, the corrected cross-sections with ISR, that is, σ_{ISR}, can be obtained from the tree cross-sections σ_{Tree} using a structure function $H(x,s)$ as follows:

$$\sigma_{ISR} = \int_0^1 dx\, H(x,s)\sigma_{Tree}\left(s(1-x)\right), \tag{3.4}$$

where s is the square of the CM energy and x is the energy fraction of an emitted photon.

The total cross-section with higher-order QED corrections to ISR can be calculated using the following function [17];

$$\sigma_{ISR} = \int_0^{k_c^2/s} dx_1 \int_0^{1-x1} dx_2\, D(x_1,s)D(x_2,s)\sigma_{Tree}\left(sx_1x_2\right). \tag{3.5}$$

The structure function $D(x,s)$, which is corresponding to square root of the radiator function, gives a probability to emit a photon with energy fraction of x at the CM energy square s. In this method, electron and positron can emit different energies, and thus finite boost of the CM system can be treated. The

structure function can be obtained as

$$\begin{aligned} D(1-x,s)^2 &= H(x,s) = \Delta_2 \beta x^{\beta-1} - \Delta_1 \beta \left(1 - \frac{x}{2}\right) \\ &\quad + \frac{\beta^2}{8}\left[-4(2-x)\log x - \frac{1+3(1-x)^2}{x}\log(1-x) - 2x\right], \end{aligned} \tag{3.6}$$

where

$$\begin{aligned} \beta &= \frac{2\alpha}{\pi}\left(\log\frac{s}{m_e^2} - 1\right), \\ \Delta_2 = 1+\delta_1, \qquad & \Delta_1 = 1+\delta_1 \\ \delta_1 &= \frac{\alpha}{\pi}\left(\frac{3}{2}\log\frac{s}{m_e^2} + \frac{\pi^2}{3} - 2\right). \end{aligned}$$

This result is obtained based on perturbative calculations of initial-state photon emission diagrams up to one-loop order.

Chapter 4

Full one-loop electroweak radiative corrections to $e^+e^- \to f\bar{f}H$ processes with beam polarization effects

4.1 Selected $e^+e^- \to f\bar{f}H$ processes

As discussed in Chapter 2, several runs will be conducted at the ILC with beam energies starting from 250 GeV, which will be and then upgrade to 1 TeV. In this work, I focused on the first run with a center-of-mass energy of 250 GeV. I discuss nine $e^+e^- \to f\bar{f}H$ processes, namely, $e^+e^- \to \mu^+\mu^-H$, e^+e^-H, $\tau^+\tau^-H$, $\nu_\mu\bar{\nu}_\mu H$, $\nu_e\bar{\nu}_e H$, $u\bar{u}H$, $d\bar{d}H$, $c\bar{c}H$, and $b\bar{b}H$. I do not discuss the $\nu_\tau\bar{\nu}_\tau H$ and $s\bar{s}H$ processes, which will be explained in later. In this chapter, I present the main findings of this thesis, that is, results obtained using the GRACE-Loop system.

First, I confirmed that our GRACE-Loop system can show the good consistency by varying the dimensional regularization parameter C_{UV}, the non-linear gauge parameters $\tilde{\alpha}, \tilde{\beta}, \tilde{\delta}, \tilde{\kappa}, \tilde{\varepsilon}$ and the fictitious photon mass λ.
By varying C_{UV} from 0 to 100 for the $e^+e^- \to \mu^+\mu^-H$ process with $k_c = 10^{-1}$ GeV and $\lambda = 10^{-17}$ GeV at $\sqrt{s} = 250$ GeV, I obtained C_{UV} independence with an agreement up tp 33 digits as shown in Table 4.1.

C_{UV}	Evaluation of the 1 loop amplitude at a phase space point
0	0.13060641075856815884748129974468 6
100	0.13060641075856815884748129974468 6

TABLE 4.1: Changing C_{UV} from 0 to 100 of $e^+e^- \to \mu^+\mu^-H$ with $k_c = 10^{-1}$ GeV and $\lambda = 10^{-17}$ GeV at $\sqrt{s} = 250$ GeV.

Non-linear gauge parameter independence was confirmed by varying $\tilde{\alpha}, \tilde{\beta}, \tilde{\delta}, \tilde{\kappa}, \tilde{\varepsilon}$ from $(0, 0, 0, 0, 0)$ to $(10, 20, 30, 40, 50)$ with $C_{UV} = 100$, which resulted in an agreement up to 15 digits as shown in Table 4.2.

$\tilde{\alpha}, \tilde{\beta}, \tilde{\delta}, \tilde{\kappa}, \tilde{\varepsilon}$	Evaluation of the 1 loop amplitude at a phase space point
0,0,0,0,0	0.13060641075856815884748129974468 6
10,20,30,40,50	0.13060641075856849191438868729164 8

TABLE 4.2: Non-linear gauge parameters independence by changing $\tilde{\alpha}, \tilde{\beta}, \tilde{\delta}, \tilde{\kappa}, \tilde{\varepsilon}$ from (0,0,0,0,0) to (10,20,30,40,50) of $e^+e^- \to \mu^+\mu^- H$ with $k_c = 10^{-1}$ GeV and $\lambda = 10^{-17}$ GeV at $\sqrt{s} = 250$ GeV

Fictitious photon mass independence was achieved by varying λ from 10^{-17} GeV to 10^{-19} GeV with $C_{UV} = 100$ has up to 14-digit agreement as shown in Table 4.3. Next, I discuss the k_c independence of all nine processes ($\mu^+\mu^- H$,

λ [GeV]	Evaluation of the 1 loop amplitude at a phase space point
10^{-17}	0.13060641075856815884748129974468 6
10^{-19}	0.13060641075856924131493030927231 3

TABLE 4.3: λ independence by changing from 10^{-17} GeV to 10^{-19} GeV with $C_{UV} = 100$ and with $k_c = 10^{-1}$ GeV of $e^+e^- \to \mu^+\mu^- H$ at $\sqrt{s} = 250$ GeV

$e^+e^- H$, $\tau^+\tau^- H$, $\nu_\mu\bar{\nu}_\mu H$, $\nu_e\bar{\nu}_e H$, $u\bar{u}H$, $d\bar{d}H$, $c\bar{c}H$, $b\bar{b}H$) without polarization. To achieve k_c independence, phase-space integration must be performed to obtain the total cross-sections. For this, I used the adaptive Monte Carlo integration package of the BASES [18]. In the BASES operation, I set 10 iteration steps for the grid optimization and 50 iteration steps for the accumulation with 40,000 sampling point to integrate one-loop amplitude, it takes 4.5 hours for $\mu^+\mu^- H$ and other processes; almost 52 hours for $b\bar{b}H$ with 16 Xeon 3.20 GHz CPU with the size of memory 128 GB. The typical integration errors are 0.01% for the loop calculation.

It should be noted that in the FULL model, all of the couplings of the scalar particles such as the Higgs boson or pseudo-Goldstone scalar bosons and fermions in the SM are included. On the contrary, I define the NOLLS approximation which has the NOn Light-fermion Light-fermion Scalar coupling except for bottom quark and top quark. In this work, the bottom- and top quark are considered to be heavy fermions and other fermions are recognized to be light ones. When the two cases are compared, the number of tree diagrams and one-loop Feynman diagrams in the FULL model were found to be much larger than in the NOLLS approximation; thus, the integration over phase space is not practical in the former, as shown in Table 4.5.
From Table 4.5, we observe that the number of one-loop Feynman diagrams

	the NOLLS approximation			the FULL model		
Graph information	one-loop	Tree	5-point	one-loop	Tree	5-point
$\mu^+\mu^-H$	208	1	10	2235	21	170
e^+e^-H	416	2	20	4470	42	340
$\tau^+\tau^-H$	208	1	28	2235	21	188
$\nu_\mu\bar{\nu}_\mu H$	122	1	6	604	4	36
$\nu_e\bar{\nu}_e H$	219	2	15	1350	12	113
$u\bar{u}H$	209	1	10	2327	21	174
$d\bar{d}H$	209	1	10	2327	21	174
$c\bar{c}H$	209	1	10	2327	21	174
$b\bar{b}H$	651	6	29	2327	21	193

TABLE 4.4: The numbers of Feynman diagrams for the NOLLS approximation and the FULL model of nine processes

	the NOLLS approx.		the FULL model	
Processes	one-loop	Tree	one-loop	Tree
$\mu^+\mu^-H$	208	1	2235	21
e^+e^-H	416	2	4470	42
$\tau^+\tau^-H$	208	1	2235	21
$\nu_\mu\bar{\nu}_\mu H$	122	1	604	4
$\nu_e\bar{\nu}_e H$	219	2	1350	12
$u\bar{u}H$	209	1	2327	21
$d\bar{d}H$	209	1	2327	21
$c\bar{c}H$	209	1	2327	21
$b\bar{b}H$	651	6	2327	21

TABLE 4.5: Numbers of Feynman diagrams between the NOLLS approximation and the FULL model of nine processes

for the $\mu^+\mu^-H$ and $\tau^+\tau^-H$ processes is the same, with 208 and 2235 diagrams with the NOLLS approximation and the FULL model, respectively. Similarly, the number of one-loop Feynman diagrams for $u\bar{u}H$ and $c\bar{c}H$ processes is the same, with 209 and 2327 diagrams according to one-loop level with the NOLLS approximation and the FULL model, respectively. However, numbers of Feynman diagrams at one-loop for $d\bar{d}H$ are 209 at the NOLLS approximation and 2327 at the FULL model; numbers of Feynman diagrams one-loop for $b\bar{b}H$ are 651 at the NOLLS approximation and 2327 at the FULL model.

Therefore the first check is to see the agreement between the FULL model and the NOLLS approximation at one phase space point. It should be noticed that the non-linear gauge independence is destroyed due to the missing of LLS (light light fermion scalar) couplings in the NOLLS approximation.

You also see the four-digit agreement between the FULL model and NOLLS approximation for the 1 loop amplitude at a phase space point at the Table 4.6. This accuracy is good enough for the phase space integration because

the error of the Monte-Carlo integration is approximately 0.1% To confirm

	Evaluation of the 1 loop amplitude at a phase space point
FULL	0.13060641075856815884748129974468 6
NOLLS	0.13065443376398261365878283868369 2

TABLE 4.6: Evaluation of the 1 loop amplitude at a phase space point for the $e^+e^- \to \mu^+\mu^- H$ with $k_c = 10^{-1}$ GeV at $\sqrt{s} = 250$ GeV

the k_c independence, I compare the total ratio δ_{Total} with various k_c values: $k_c = 10^{-1}$ GeV, $k_c = 10^{-3}$ GeV and $k_c = 10^{-5}$ GeV where the cross-sections for the NOLLS approximation is the sum of cross-sections at the tree level, Loop, Soft and Hard photon.

$$\begin{aligned}\sigma_{\mathcal{O}_\alpha} &= \sigma_{Tree} + \sigma_{Loop} + \sigma_{Soft} + \sigma_{Hard} \\ &= \sigma_{Tree} + \sigma_{Loop}(C_{UV}, \lambda, \tilde{\alpha}, \tilde{\beta}, \tilde{\delta}, \tilde{\epsilon}, \tilde{\kappa}) + \sigma_{Tree}\delta_{soft}(\lambda, E_\gamma < k_c) + \sigma_{Hard}(k_c)\end{aligned}$$

as in Eq 3.1.
The total ratio between $\mathcal{O}_\alpha$ correction and the tree level cross-sections

$$\delta_{Total} = \left(\frac{\sigma_{\mathcal{O}_\alpha}}{\sigma_{Tree}} - 1\right) \times 100. \tag{4.1}$$

	$\delta_{Total}(\%)$		
Processes	$k_c = 10^{-1}$ GeV	$k_c = 10^{-3}$ GeV	$k_c = 10^{-5}$ GeV
$\mu^+\mu^- H$	not converged	-4.039	-4.017
$e^+e^- H$	-4.850	-4.807	-4.787
$\tau^+\tau^- H$	-3.642	-3.731	-3.787
$\nu_\mu\bar{\nu}_\mu H$	-4.294	-4.302	-4.298
$\nu_e\bar{\nu}_e H$	-3.341	-3.332	-3.328
$u\bar{u}H$	-6.754	-6.826	-6.763
$d\bar{d}H$	-4.554	-4.605	-4.773
$c\bar{c}H$	-6.763	-6.875	-6.770
$b\bar{b}H$	-6.110	-6.163	-6.247

TABLE 4.7: δ_{Total} with various k_c values: $k_c = 10^{-1}$ GeV, $k_c = 10^{-3}$ GeV and $k_c = 10^{-5}$ GeV for all nine processes ($\mu^+\mu^- H$, $e^+e^- H$, $\tau^+\tau^- H$, $\nu_\mu\bar{\nu}_\mu H$, $\nu_e\bar{\nu}_e H$, $u\bar{u}H$, $d\bar{d}H$, $c\bar{c}H$, $b\bar{b}H$) without polarization at $\sqrt{s} = 250$ GeV.

The difference in percentage of the total ratios δ_{Total} with $k_c = 10^{-3}$ GeV and $k_c = 10^{-5}$ GeV without polarization at $\sqrt{s} = 250$ GeV is shown in Table 4.9.
Here, I define $\Delta(\%) = \delta_{Total_{k_c=10^{-3}\text{GeV}}} - \delta_{Total_{k_c=10^{-5}\text{GeV}}}$.

	$\delta_{Total}(\%)$	
Processes	$k_c = 10^{-3}$ GeV	$k_c = 10^{-5}$ GeV
$\mu^+\mu^-H$	-4.039	-4.017
e^+e^-H	-4.807	-4.787
$\tau^+\tau^-H$	-3.731	-3.787
$\nu_\mu\bar{\nu}_\mu H$	-4.302	-4.298
$\nu_e\bar{\nu}_e H$	-3.332	-3.328
$u\bar{u}H$	-6.826	-6.763
$d\bar{d}H$	-4.605	-4.773
$c\bar{c}H$	-6.875	-6.770
$b\bar{b}H$	-6.163	-6.247

TABLE 4.8: δ_{Total} with various k_c values: $k_c = 10^{-1}$ GeV, $k_c = 10^{-3}$ GeV and $k_c = 10^{-5}$ GeV for all nine processes ($\mu^+\mu^-H$, e^+e^-H, $\tau^+\tau^-H$, $\nu_\mu\bar{\nu}_\mu H$, $\nu_e\bar{\nu}_e H$, $u\bar{u}H$, $d\bar{d}H$, $c\bar{c}H$, $b\bar{b}H$) without polarization at $\sqrt{s} = 250$ GeV.

Processes	$\Delta(\%)$
$\mu^+\mu^-H$	-0.022
e^+e^-H	-0.020
$\tau^+\tau^-H$	-0.054
$\nu_\mu\bar{\nu}_\mu H$	-0.001
$\nu_e\bar{\nu}_e H$	-0.004
$u\bar{u}H$	-0.063
$d\bar{d}H$	0.169
$c\bar{c}H$	-0.105
$b\bar{b}H$	0.084

TABLE 4.9: The difference in percentage of the total ratio δ_{Total} and $k_c = 10^{-5}$ GeV without polarization at $\sqrt{s} = 250$ GeV.

With the above results, one can see that the least accurate is for $d\bar{d}H$ with 0.169% thus I can guarantee of the accuracy of my $O(\alpha)$ calculations approximately 0.2% for all processes.

Now I am going to show five types of typical one-loop Feynman diagrams in three-point Fig. 4.1, four-point, five-point function Fig. 4.2 and fish type Fig. 4.3 Feynman diagrams of $e^+e^- \to \mu^+\mu^-H$ which are discussed in detail in [19].

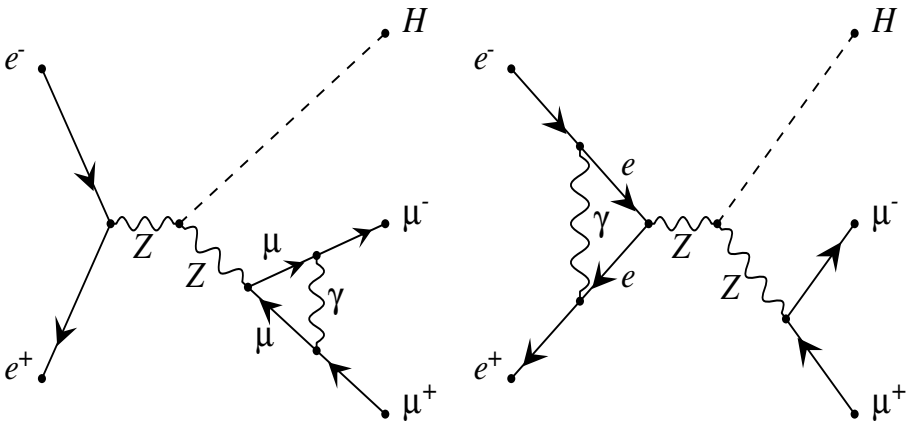

FIGURE 4.1: Typical final and initial vertex correction Feynman diagrams of $e^+e^- \to \mu^+\mu^- H$

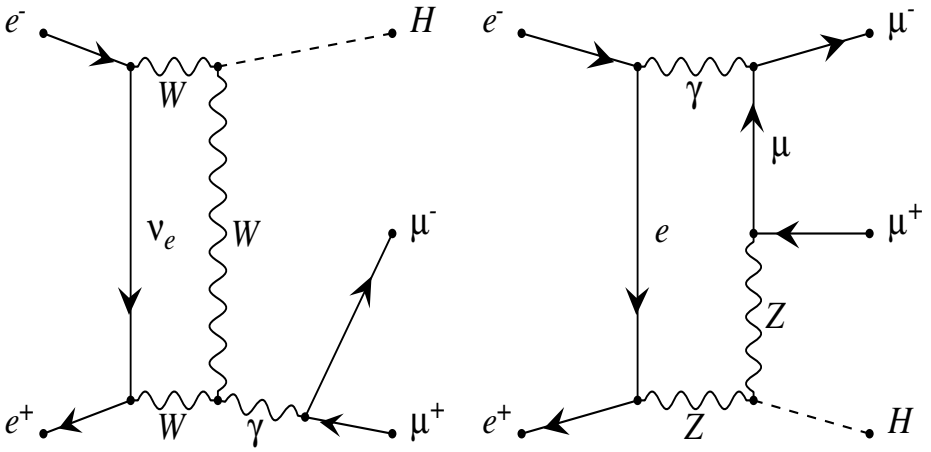

FIGURE 4.2: Typical 4 point and 5 point function Feynman diagrams of $e^+e^- \to \mu^+\mu^- H$

Next, I compare the unpolarized cross-sections of $e^+e^- \to \nu\bar{\nu}H$ at the center-of-mass energy $\sqrt{s} = 500$ GeV. I denote "Current" for current work and [20] for previous work. The comparison is presented in Table 4.20. I observed that the consistent results in the integration errosr for all cases. I list for each Higgs-boson mass and the corresponding calculated W-boson mass calculated by German group together with my current results. I observed that the agreement is good. The correction factors (δ_{Total}) to the lowest-order cross-sections agree within 0.3%.

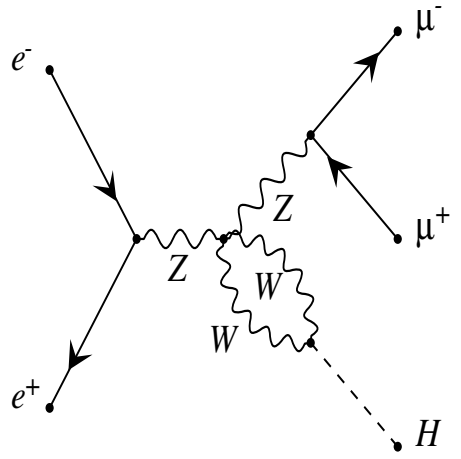

FIGURE 4.3: Typical Fish Feynman diagram of $e^+e^- \to \mu^+\mu^- H$

M_H (GeV)	M_W (GeV)	σ_{Tree} (pb)	$\sigma_{\mathcal{O}_\alpha}$ (pb)	δ_{Total}%	
150	80.3767	6.1072(9)E-02	6.075(6)E-02	-0.51	Current
		6.1076(5)E-02	6.080(2)E-02	-0.44	Ref.[20]
200	80.3571	3.7302(5)E-02	3.703(4)E-02	-0.71	Current
		3.7293(3)E-02	3.709(2)E-02	-0.56	Ref.[20]
250	80.3411	2.110(2)E-02	2.059(2)E-02	-2.42	Current
		2.1134(1)E-02	2.060(1)E-02	-2.53	Ref.[20]
300	80.3275	1.0744(7)E-02	1.0258(7)E-02	-4.51	Current
		1.07552(7)E-02	1.0282(4)E-02	-4.40	Ref.[20]
350	80.3158	4.6077(4)E-03	4.172(2)E-03	-9.46	Current
		4.6077(2)E-03	4.181(1)E-03	-9.27	Ref.[20]

TABLE 4.10: Comparison between the unpolarized cross-sections of $e^+e^- \to \nu\bar{\nu}H$ between the current results and those of German group
at center-of-mass energy $\sqrt{s} = 500$ GeV.

4.2 Lepton processes with the polarization

4.2.1 $e^+e^- \to \mu^+\mu^- H$

Table 4.11 shows the cross-sections of the tree level, the cross-sections for the NOLLS approximation and those of ISR effects, total ratios for the NOLLS approximation and those with the ISR effects for various polarization conditions (i.e., UP, RR, LL, RL, LR and ILC) which are defined in Chapter 2.

The total cross section for the NOLLS approximation is the sum of cross-

	σ_{Tree} (pb)	$\sigma_{\mathcal{O}_\alpha}$ (pb)	δ_{Total}%	σ_{ISR} (pb)	δ_{ISR}%
UP	7.041(7)E-03	6.756(6)E-03	-4.04E+00	6.326(4)E-03	-1.02E+01
RR	2.16(1)E-11	8.4(2)E-07	3.91E+06	9.62(3)E-13	4.44E+05
LL	2.16(1)E-11	8.45(2)E-07	3.91E+06	7(2)E-11	3.72E+05
RL	1.108(1)E-02	1.196(1)E-02	7.71E+00	9.94(2)E-03	-1.02E+01
LR	1.709(2)E-02	1.504(1)E-02	-1.20E+01	1.534(3)E-02	-1.02E+01
ILC	1.039(8)E-02	9.200(1)E-03	-1.14E+01	9.320(4)E-03	-1.03E+01

TABLE 4.11: The cross section of $e^+e^- \to \mu^+\mu^- H$ with various conditions of the beam polarization and without experimental cuts.

sections at the tree level, Loop, Soft and Hard photon after applying the experimental cut and polarization 30% for e_R^+ and 80% for e_L^-.

$$\sigma_{\mathcal{O}_\alpha} = \sigma_{Tree} + \sigma_{Loop} + \sigma_{Soft} + \sigma_{Hard} \tag{4.2}$$

The total ratio between $\mathcal{O}_\alpha$ correction and the tree level cross-sections

$$\delta_{Total} = \left(\frac{\sigma_{\mathcal{O}_\alpha}}{\sigma_{Tree}} - 1\right) \times 100. \tag{4.3}$$

In the s-channel, Z boson has spin 1. LL and RR collisions can not form spin-1 state, but I keep the electron mass then the spin flipping can occur to form spin-1 state. The amplitude must have terms $\left|\frac{m_e^2}{s}\right| \propto \left(\frac{10^{-3}}{10^2}\right)^2 \sim 10^{-10}$ that is why cross section of LL and RR have the order of 10^{-11}. The cross-sections of LL and RR at the tree level are very small but still exist as you can see in Table 4.11. For LL and RR, you will see large total ratio $\delta_{Total} \sim 10^6$ because of the radiation effect. Unfortunately it cannot be observed directly in the experiments. However the ILC experiment includes this effect so it should be noticed.

$\sigma_{\mathcal{O}_\alpha ILC\mu^+\mu^- H} = 1.039(8) \times 10^{-2}$ pb is larger than $\sigma_{\mathcal{O}_\alpha UP\mu^+\mu^- H} = 7.041(7) \times 10^{-3}$ pb thanks to the advantages of the beam polarization of the linear collider. It has significantly better statistics of Higgs with the same luminosity.

The difference between δ_{Total} and δ_{ISR} is approximately 1%. δ_{Total} includes the effect electroweak one-loop corrections but δ_{ISR} is the result of high order QED corrections. It is not easy to confirm which one is more important but one should know this point.

4.2.2 $e^+e^- \to e^+e^- H$

Note that the notations and symbols used for the $e^+e^- \to e^+e^- H$ and other processes are the same as those for the $e^+e^- \to \mu^+\mu^- H$ process, for the UP, RR, LL, RL, LR, and ILC. In this process, because of sizable t-channel amplitude contribution, $\sigma_{\mathcal{O}_\alpha ILCe^+e^- H} = 9.919(2) \times 10^{-3}$ pb is larger than

$\sigma_{\mathcal{O}_\alpha ILC\mu^+\mu^- H} = 9.200(1) \times 10^{-3}$ pb in section **4.2.1** approximately 1% at the proposed ILC because of sizable t-channel amplitude contribution. Because it is not needed to form spin-1 state at t-channel, LL and RR cross-sections are sizable even at the tree level. Table 4.12 shows detailed values.

	σ_{Tree} (pb)	$\sigma_{\mathcal{O}_\alpha}$ (pb)	δ_{Total}%	σ_{ISR} (pb)	δ_{ISR}%
UP	7.731(1)E-03	7.360(1)E-03	-4.81E+00	1.583(1)E-03	-7.95E+01
RR	6.87(4)E-04	6.22(1)E-04	-9.52E+00	7.71(4)E-05	-8.88E+01
LL	6.87(4)E-04	6.2(3)E-04	-9.41E+00	3.09(2)E-04	-8.88E+01
RL	1.149(2)E-02	1.235(1)E-02	7.53E+00	2.443(5)E-03	-7.87E+01
LR	1.806(3)E-02	1.580(2)E-02	-1.25E+01	3.734(8)E-03	-7.93E+01
ILC	1.123(9)E-02	9.919(2)E-03	-1.17E+01	9.196(4)E-03	-1.81E+01

TABLE 4.12: The cross section of $e^+e^- \to e^+e^-H$ with various conditions of the beam polarization and without experimental cuts.

4.2.3 $e^+e^- \to \tau^+\tau^-H$

There is a question about tau particle which we are interested in: whether the tau mass can be neglected or not.

$\sigma_{\mathcal{O}_\alpha ILC\tau^+\tau^- H} = 9.309(2) \times 10^{-3}$ pb and $\sigma_{\mathcal{O}_\alpha ILC\mu^+\mu^- H} = 9.2100(1) \times 10^{-3}$ pb in section **4.2.1** are quite similar as we expected because all of final radiation effects like $ln\left(\frac{m_\tau^2}{s}\right)$ are canceled of each other according to the Kinoshita-Lee-Nauenberg theorem [21, 22]. The terms from the initial state radiation of $ln\left(\frac{m_e^2}{s}\right)$ of e^+e^- still remains. More numbers will be shown in Table 4.13.

	σ_{Tree} (pb)	$\sigma_{\mathcal{O}_\alpha}$ (pb)	δ_{Total}%	σ_{ISR} (pb)	δ_{ISR}%
UP	7.037(7)E-03	6.774(7)E-03	-3.73E+00	5.573(1)E-03	-2.08E+01
RR	2.10(2)E-09	8.44(3)E-07	4.02E+04	8.20(7)E-12	-9.96E+01
LL	2.10(2)E-09	8.44(3)E-07	4.01E+04	8.3(7)E-12	-9.96E+01
RL	1.107(1)E-02	1.193(6)E-02	7.45E+00	9.944(2)E-03	6.32E+04
LR	6.311(4)E-02	1.520(1)E-02	-1.10E+01	6.311(1)E-02	1.16E+04
ILC	1.038(8)E-02	9.309(2)E-03	-1.03E+01	9.299(4)E-03	-1.04E+01

TABLE 4.13: The cross section of $e^+e^- \to \tau^+\tau^-H$ with various conditions of the beam polarization and without experimental cuts.

4.2.4 $e^+e^- \to \nu_\mu \bar{\nu}_\mu H$

The difference between δ_{Total} and δ_{ISR} is approximately 1%. I skip $e^+e^- \to \nu_\tau \bar{\nu}_\tau H$ process because it is quite similar to this one. Table 4.14 provides us more data.

	σ_{Tree} (pb)	$\sigma_{\mathcal{O}_\alpha}$ (pb)	δ_{Total}%	σ_{ISR} (pb)	δ_{ISR}%
UP	1.392(2)E-02	1.332(3)E-02	-4.30E+00	1.25(1)E-02	-1.01E+01
RR	2.71(1)E-12	1.669(7)E-06	6.16E+07	1.971(6)E-12	-2.73E+01
LL	2.71(1)E-12	1.669(7)E-06	6.15E+07	2.307(7)E-12	-1.49E+01
RL	2.190(8)E-02	2.414(7)E-02	1.02E+01	1.965(6)E-02	-1.03E+01
LR	3.377(1)E-02	2.914(1)E-02	-1.37E+01	3.034(1)E-02	-1.02E+01
ILC	2.053(2)E-02	1.790(1)E-02	-1.28E+01	1.845(1)E-02	-1.02E+01

TABLE 4.14: The cross section of $e^+e^- \to \nu_\mu \bar{\nu}_\mu H$ with various conditions of the beam polarization and without experimental cuts.

4.2.5 $e^+e^- \to \nu_e \bar{\nu}_e H$

$e^+e^- \to \nu_e \bar{\nu}_e H$ has t-channel. Table 4.15 shows the results of $e^+e^- \to \nu_e \bar{\nu}_e H$ process.

	σ_{Tree} (pb)	$\sigma_{\mathcal{O}_\alpha}$ (pb)	δ_{Total}%	σ_{ISR} (pb)	δ_{ISR}%
UP	2.071(9)E-02	2.002(9)E-02	-3.33E+00	1.74(2)E-02	-1.59E+01
RR	3.05(2)E-12	3.53(2)E-06	1.16E+08	2.043(8)E-12	-3.30E+01
LL	3.05(2)E-12	3.53(2)E-06	1.16E+08	2.385(9)E-12	-2.18E+01
RL	2.190(8)E-02	2.414(7)E-02	1.02E+01	1.925(6)E-02	-1.21E+01
LR	6.09(4)E-02	5.614(2)E-02	-7.89E+00	5.031(2)E-02	-1.74E+01
ILC	3.641(5)E-02	3.336(3)E-02	-8.80E+00	3.221(2)E-02	-1.73E+01

TABLE 4.15: The cross section of $e^+e^- \to \nu_e \bar{\nu}_e H$ with various conditions of the beam polarization and without experimental cuts.

4.3 Quark processes

4.3.1 $e^+e^- \to u\bar{u}H$

QCD corrections up to 4-loop level is well known, and with just in one-loop corrections is popular as the simple factor of $1 + \frac{\alpha_s}{\pi} \simeq 1.03\%$, where α_s is the coupling constant of the strong interaction $(\alpha_s \simeq 1/10)$ thus I will not discuss about it in my thesis. Table 4.16 shows calculation results of the first quark process $e^+e^- \to u\bar{u}H$.

	σ_{Tree} (pb)	$\sigma_{\mathcal{O}_\alpha}$ (pb)	δ_{Total}%	σ_{ISR} (pb)	δ_{ISR}%
UP	2.431(3)E-02	2.265(1)E-02	-6.76E+00	2.185(2)E-02	-1.13E+01
RR	3.65(2)E-11	2.915(1)E-06	7.98E+06	8.(4)E-11	1.30E+02
LL	3.65(2)E-11	2.92(1)E-06	7.98E+06	8.(4)E-11	1.31E+02
RL	3.825(1)E-02	4.310(3)E-02	1.28E+01	5.298(3)E-02	-1.10E+01
LR	5.899(2)E-02	5.899(2)E-02	-1.92E+01	3.433(8)E-02	-1.10E+01
ILC	3.586(3)E-02	2.948(4)E-02	-1.80E+01	3.221(2)E-02	-1.02E+01

TABLE 4.16: The cross section of $e^+e^- \to u\bar{u}H$ with various conditions of the beam polarization and without experimental cuts.

4.3.2 $e^+e^- \to d\bar{d}H$

The iso-spin of u quark is up, on the other hand, the iso-spin of d quark is down, which explains the difference between $\sigma_{\mathcal{O}_\alpha ILCd\bar{d}H} = 3.970(6) \times 10^{-2}$ pb and $\sigma_{\mathcal{O}_\alpha ILCu\bar{u}H} = 2.948(4) \times 10^{-2}$ pb as in section **4.3.1**. Table 4.17 shows the results of $e^+e^- \to d\bar{d}H$ process.

	σ_{Tree} (pb)	$\sigma_{\mathcal{O}_\alpha}$ (pb)	δ_{Total}%	σ_{ISR} (pb)	δ_{ISR}%
UP	3.119(4)E-02	2.98(2)E-02	-4.61E+00	2.803(5)E-02	-1.01E+01
RR	1.40(1)E-11	3.74(2)E-06	2.67E+07	1.9(8)E-10	1.24E+03
LL	1.40(1)E-11	3.74(2)E-06	2.68E+07	1.8(8)E-10	1.19E+03
RL	7.567(3)E-02	5.205(4)E-02	6.08E+00	4.404(3)E-02	-1.03E+01
LR	4.907(2)E-02	6.650(4)E-02	-1.21E+01	6.798(4)E-02	-1.02E+01
ILC	4.600(5)E-02	3.970(6)E-02	-1.37E+01	4.132(2)E-02	-1.02E+01

TABLE 4.17: The cross section of $e^+e^- \to d\bar{d}H$ with various conditions of the beam polarization and without experimental cuts.

4.3.3 $e^+e^- \to c\bar{c}H$

Table 4.18 shows the cross-sections of $e^+e^- \to c\bar{c}H$. The mass of charm quark is 1.5 Ge V and the mass of up quark is 58 MeV. Because there is no large mass effect from the final state radiation, the results are quite similar as expected. Because of above observation, I skip $e^+e^- \to s\bar{s}H$ process because this process has the same characteristic of $e^+e^- \to d\bar{d}H$ process.

	σ_{Tree} (pb)	$\sigma_{\mathcal{O}_\alpha}$ (pb)	δ_{Total}%	σ_{ISR} (pb)	δ_{ISR}%
UP	2.427(3)E-02	2.260(1)E-02	-6.76E+00	2.181(2)E-02	-1.01E+01
RR	1.482(7)E-11	2.91(1)E-06	1.96E+07	1.4155(8)E-11	-4.46E+00
LL	1.482(7)E-11	2.91(1)E-06	1.96E+07	1.4600(8)E-11	-1.49E+00
RL	3.819(1)E-02	4.303(2)E-02	1.26E+01	3.427(7)E-02	-1.03E+01
LR	5.891(1)E-02	4.763(4)E-02	-1.91E+01	5.297(1)E-02	-1.02E+01
ILC	3.580(3)E-02	2.940(4)E-02	-1.78E+01	3.215(2)E-02	-1.02E+01

TABLE 4.18: The cross section of $e^+e^- \to c\bar{c}H$ with various conditions of the beam polarization and without experimental cuts.

4.3.4 $e^+e^- \to b\bar{b}H$

Table 4.19 summaries cross-sections of $e^+e^- \to b\bar{b}H$. I keep the bottom-Yukawa coupling with NOLLS approximation for $e^+e^- \to b\bar{b}H$ but not in other processes. Let's compare the results of $e^+e^- \to d\bar{d}H$ and $e^+e^- \to b\bar{b}H$ of the proposed ILC at the $\mathcal{O}_\alpha$. The different is approximately 1% due to the bottom-Yukawa coupling which we are excited to know. With ISR the results for $e^+e^- \to d\bar{d}H$ and $e^+e^- \to b\bar{b}H$ are quite similar. The difference between δ_{Total} and σ_{ISR} is very interesting. Because this 1% difference originated from

	σ_{Tree} (pb)	$\sigma_{\mathcal{O}_\alpha}$ (pb)	δ_{Total}%	σ_{ISR} (pb)	δ_{ISR}%
UP	3.085(4)E-02	2.90(1)E-02	-6.16E+00	2.673(6)E-02	-1.33E+01
RR	7.40(4)E-12	3.69(2)E-06	4.99E+07	5.70(3)E-12	-2.29E+01
LL	7.40(4)E-12	3.69(2)E-06	4.99E+07	6.31(3)E-12	-1.46E+01
RL	4.853(2)E-02	5.075(4)E-02	4.56E+00	4.201(1)E-02	-1.34E+01
LR	7.485(3)E-02	7.485(3)E-02	-1.34E+01	6.483(2)E-02	-1.34E+01
ILC	4.550(5)E-02	3.974(6)E-02	-1.26E+01	4.093(2)E-02	-1.01E+01

TABLE 4.19: The cross section of $e^+e^- \to b\bar{b}H$ with various conditions of the beam polarization and without experimental cuts.

the bottom-Yukawa coupling of the bottom quark, though it may be hard to observe at the experiments.

4.4 Recoil mass distribution of $e^+e^- \to \mu^+\mu^- H$ with beam polarization effects

In this section, I discuss the ZH recoil mass distribution $ZH \to \mu^+\mu^- H$ with $\mathcal{O}(\alpha)$ corrections and beam polarization effects. To conduct a more realistic analysis, I apply the following three experimental cuts:
1. The angular cuts on $\theta_{\mu^+}, \theta_{\mu^-}$

$$10^o < \theta_{\mu^+}, \theta_{\mu^-} < 170^o, \tag{4.4}$$

where θ_{μ^+} and θ_{μ^-} are the scattering angles of anti-muon and muon, respectively.
2. The energy cuts on E_{μ^+}, E_{μ^-}

$$E_{\mu^+}, E_{\mu^-} > 10 \text{ GeV}, \tag{4.5}$$

where E_{μ^+} and E_{μ^-} are the energies of anti-muon and muon, respectively.
3. The invariant mass cut $M_{\mu^+\mu^-}$

$$m_Z - 3\Gamma_Z < M_{\mu^+\mu^-} < m_Z + 3\Gamma_Z. \tag{4.6}$$

where $M_{\mu^+\mu^-}$ is the invariant mass of anti-muon and muon particles; $\Gamma_Z = 2.49$ GeV [15] is the width of the Z-boson.
Next, I present the results of the ZH recoil mass distribution with the $\mathcal{O}(\alpha)$ corrections of $e^+e^- \to \mu^+\mu^- H$ at $\sqrt{s} = 250$ GeV, after applying the three types of experimental cuts as defined above. The recoil mass distribution is shown in Fig. 4.4.
The black line shows the tree level distribution, the blue line shows the ISR

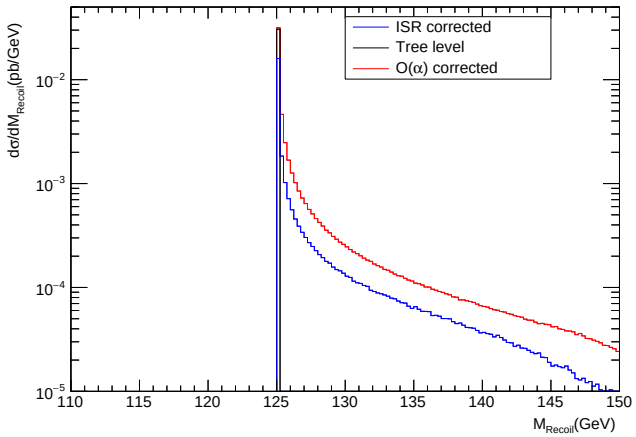

FIGURE 4.4: Recoil mass distribution of $e^+e^- \to \mu^+\mu^- H$ after applying the experimental cuts as in Eqs (4.3), (4.4),(4.5) at $\sqrt{s} =$ 250 GeV. The bin width is 0.3 GeV.

corrected distribution and the red line shows the $\mathcal{O}(\alpha)$ corrected distribution. The black line only shows the one bin peak and of which position indicates the mass of Higgs boson. On including the $\mathcal{O}(\alpha)$ corrections, a tail structure appears owing to the ISR effects, which is called the radiative tail. The height of peak is substantially reduced owing to the one-photon emission effect. However, the ISR effects are included, the height of the peak increases again because of the higher-order radiation effect. This swing back effect can be seen, occasionally when comparing the higher-order and $\mathcal{O}(\alpha)$ corrections.

After applying the three experimental cuts, I obtained the total cross-sections at $\mathcal{O}(\alpha)$ and those including ISR effects and the total ratios at $\mathcal{O}(\alpha)$ and those including ISR effects as shown in Table 4.20 From this table, I see

σ_{Tree} (pb)	$\sigma_{\mathcal{O}_\alpha}$ (pb)	σ_{ISR} (pb)	$\delta_{\mathcal{O}_\alpha}$%	δ_{ISR}%
9.55E-03	7.94E-03	8.24E-03	-16.9	-13.8

TABLE 4.20: Summary table of cross-sections and total ratios of $e^+e^- \to \mu^+\mu^- H$ with experimental cuts and with ILC proposed polarization $p_e = -0.8$, $p_p = 0.3$.

that the total ratio at $\mathcal{O}(\alpha)$ is -16.9% and the total ratio with the ISR effects is -13.8%. The difference is approximately 3%. The analysts might be interested in this finding, especially the bottom quark case.

Chapter 5

Conclusion

In this thesis, I performed three kinds of tests on the GRACE-Loop system to confirm that the amplitudes are independent of all redundant parameters at random phase-space points before calculating all the cross-sections. These tests checked

1. the finiteness of the result in the absence of the ultraviolet coefficient C_{UV},
2. IR finiteness by introducing a fictitious photon mass parameter λ,
3. non-linear-gauge parameter independence, which was performed using a set of five-gauge-fixing parameters- $\tilde{\alpha}, \tilde{\beta}, \tilde{\delta}, \tilde{\kappa}$, and $\tilde{\varepsilon}$.

I introduced the NOLLS approximation and also confirmed its accuracy. In addition to the above checks, I checked the hard photon cut-off k_c independence, which had a precision within 0.2% for all the processes. Using NOLLS approximation, I calculated the total cross-sections and total ratios at the $\mathcal{O}(\alpha)$ corrections and those by including ISR effects for nine $e^+e^- \to f\bar{f}H$ processes $\mu^+\mu^-H$, e^+e^-H, $\tau^+\tau^-H$, $\nu_\mu\bar{\nu}_\mu H$, $\nu_e\bar{\nu}_e H$, $u\bar{u}H$, $d\bar{d}H$, $c\bar{c}H$, $b\bar{b}H$ for various beam polarization conditions (i.e., UP, RR, LL, RL, LR, and ILC).

First, I discuss the behavior of high-order corrections for the $e^+e^- \to \mu^+\mu^-H$ process in detail. For this process, various conditions of beam polarization without experimental cuts are shown in Table 5.1. At the tree level,

	σ_{Tree} (pb)	$\sigma_{\mathcal{O}_\alpha}$ (pb)	δ_{Total}%	σ_{ISR} (pb)	δ_{ISR}%
UP	7.041(7)E-03	6.756(6)E-03	-4.04E+00	6.326(4)E-03	-1.02E+01
RR	2.16(1)E-11	8.4(2)E-07	3.91E+06	9.62(3)E-13	4.44E+05
LL	2.16(1)E-11	8.45(2)E-07	3.91E+06	7(2)E-11	3.72E+05
RL	1.108(1)E-02	1.196(1)E-02	7.71E+00	9.94(2)E-03	-1.02E+01
LR	1.709(2)E-02	1.504(1)E-02	-1.20E+01	1.534(3)E-02	-1.02E+01
ILC	1.039(8)E-02	9.200(1)E-03	-1.14E+01	9.320(4)E-03	-1.03E+01

TABLE 5.1: The cross section of $e^+e^- \to \mu^+\mu^-H$ with various conditions of the beam polarization and without experimental cuts.

the cross-sections corresponding to the RR and LL are negligibly small compared with those of RL and LR since RR and LL polarizations cannot produce

spin-1 boson. Small cross-sections of RR and LL polarizations are resulted from spin-flip effect, which are propotional to $|\frac{me^2}{s}| \propto \left(\frac{10^{-3}}{10^2}\right)^2 \sim 10^{-10}$. These results are consistent with $\frac{LL+RR}{LR+RL} \sim 10^{-11}$. Moreover, $\sigma_{\mathcal{O}_\alpha}$ gives sizeable cross-sections on RR and LL polarizations, because $\mathcal{O}_\alpha$ amplitude includes spin-flip diagrams of the initial state radiation. For LL and RR, although the cross-sections of LL and RR at the tree level are very small, the very large total ratios $\delta_{Total} \sim 10^6$ are observed. $\sigma_{\mathcal{O}_\alpha ILC\mu^+\mu^- H} = 1.039(8) \times 10^{-2}$ pb is larger than $\sigma_{\mathcal{O}_\alpha UP\mu^+\mu^- H} = 7.041(7) \times 10^{-3}$ pb thanks to the advantages of the beam polarization of the linear collider. It has significantly better statistics of Higgs with the same luminosity.

Next, I discuss the effect of higher-order corrections on weak interactions and photonic interactions. Note that $\sigma_{\mathcal{O}_\alpha}$ includes both QED and weak corrections. However, it is impossible in general to clearly separate theses two effects. I calculated δ_{ISR} as an approximation for QED corrections because ISR corrections dominate over all QED corrections. In this approximation, the weak corrections can be estimated as $\sigma_{weak} = \sigma_{\mathcal{O}_\alpha} - \sigma_{ISR}$. δ_{ISRRL} and δ_{ISRLR} were both obtained to be 10.2%; however, $\delta_{TotalRL} = 7.71\%$, and $\delta_{TotalLR} = -12\%$. Thus the weak correction corresponding to RL is 17% but that corresponding to LR is only -2%. From these results, it is clear that beam polarization and precise calculations are very important. $\delta_{TotalILC} = -11.4\%$, $\delta_{ISRILC} = 10.3\%$, and the weak correction for the proposed ILC polarization is approximately 1%. This result is sufficient to motivate the ILC to consider the contribution of the weak correction. Additionally, $\sigma_{\mathcal{O}_\alpha}$ corrections are necessary to compare with a running alpha of 14%.

I summarize lepton processes $e^+e^- \to f\bar{f}H$ (i.e., $\mu^+\mu^- H$, $e^+e^- H$, $\tau^+\tau^- H$, $\nu_\mu\bar{\nu}_\mu H$, and $\nu_e\bar{\nu}_e H$) in Table 5.2 . I present two separate figures for the cross-

Processes	σ_{Tree} (pb)	$\sigma_{\mathcal{O}_\alpha}$ (pb)	δ_{Total}%	σ_{ISR} (pb)	δ_{ISR}%
$\mu^+\mu^- H$	1.039(8)E-02	9.200(1)E-03	-1.14E+01	9.320(4)E-03	-1.03E+01
$e^+e^- H$	1.123(9)E-02	9.919(2)E-03	-1.17E+01	9.196(4)E-03	-1.81E+01
$\tau^+\tau^- H$	1.038(8)E-02	9.309(2)E-03	-1.03E+01	9.299(4)E-03	-1.04E+01
$\nu_\mu\bar{\nu}_\mu H$	2.053(2)E-02	1.790(1)E-02	-1.28E+01	1.845(1)E-02	-1.02E+01
$\nu_e\bar{\nu}_e H$	3.641(5)E-02	3.336(3)E-02	-8.80E+00	3.221(2)E-02	-1.73E+01

TABLE 5.2: Lepton processes with the ILC proposed beam polarization at $\sqrt{s} = 250$ GeV and without experimental cuts.

sections and total ratios, for convenience. Fig. 5.1 shows the cross-sections at the tree level, as well as $\sigma_{\mathcal{O}_\alpha}$, and ISR cross-sections. Fig. 5.2 shows δ_{Total} and δ_{ISR} of the four leptonic processes. Owing to the sizable contribution of the t-channel amplitude, $\sigma_{\mathcal{O}_\alpha ILC\nu_e\bar{\nu}_e H} = 3.336(3) \times 10^{-2}$ pb is larger than $\sigma_{\mathcal{O}_\alpha ILC\nu\mu\bar{\nu}_\mu H} = 1.790(1) \times 10^{-2}$ pb. $\delta_{TotalILC\nu_\mu\bar{\nu}_\mu H} = -12.8\%$ and $\delta_{ISRILC\nu_\mu\bar{\nu}_\mu H} = -10.2\%$, and hence, the weak correction for $\nu_\mu\bar{\nu}_\mu H$ is approximately -3% whereas, $\delta_{TotalILC\nu_e\bar{\nu}_e H} = -8.8\%$ and $\delta_{ISRILC\nu_e\bar{\nu}_e H} = -17.3\%$,

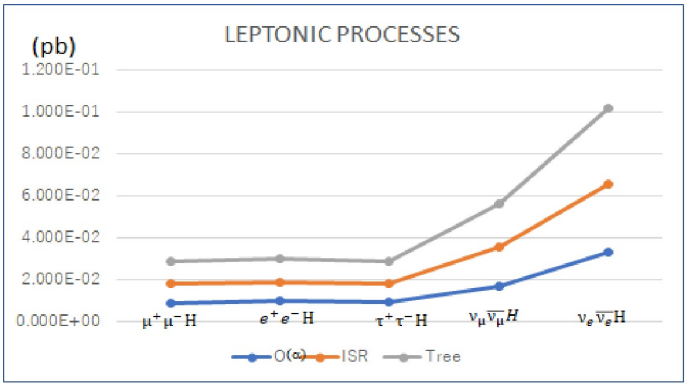

FIGURE 5.1: Cross-sections of the leptonic processes with the ILC proposed beam polarization at $\sqrt{s} = 250$ GeV and without experimental cuts.

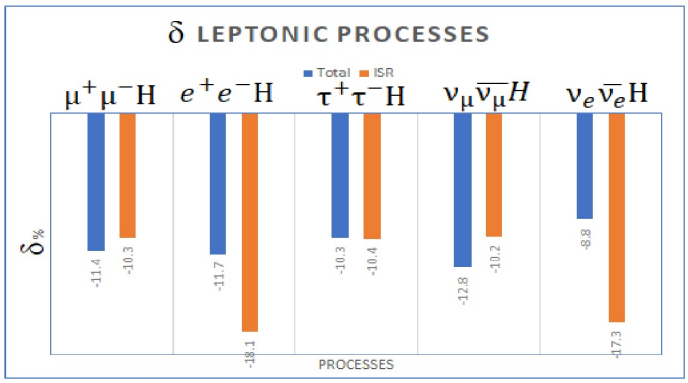

FIGURE 5.2: Ratios of the leptonic processes with the ILC proposed beam polarization at $\sqrt{s} = 250$ GeV and without experimental cuts.

hence the weak correction for $\nu_e\bar{\nu}_e H$ is approximately 8%. Moreover, $\mu^+\mu^- H$ and $e^+e^- H$ have the same tendency as $\nu_\mu\bar{\nu}_\mu H$ and $\nu_e\bar{\nu}_e H$. From this discussion, it is clear that although t-channel cross-sections at the tree level are small, they are important for $\sigma_{\mathcal{O}_\alpha}$. Tau particle is heavier than muon particle thus cross section of $\tau^+\tau^- H$ is expected to be smaller than that of $\mu^+\mu^- H$. However, $\sigma_{\mathcal{O}_\alpha ILC\tau^+\tau^- H} = 9.309(2) \times 10^{-3}$ pb is larger than $\sigma_{\mathcal{O}_\alpha ILC\mu^+\mu^- H} = 9.2100(1) \times 10^{-3}$ pb. This opposite tendency is very interesting and should be noted. $\delta_{TotalILC\nu_\mu\bar{\nu}_\mu H} = -12.8\%$ and $\delta_{TotalILC\mu^+\mu^- H} = -11.4\%$; this 1.4% difference maybe owing to the charge/neutral channel or up/down type. This finding is also interesting for further study. $\delta_{TotalILC\mu^+\mu^- H} = -11.4\%$ and $\delta_{ISR\mu^+\mu^- H} = -10.3\%$ while $\delta_{TotalILC\tau^+\tau^- H} = -10.3\%$, and $\delta_{ISRILC\tau^+\tau^- H} = -10.4\%$. Furthermore, the weak correction for $\tau^+\tau^- H$ is only 0.1%, but the weak correction for $\mu^+\mu^- H$ is 1.1%.

Next, I discuss the quark processes. $e^+e^- \to f\bar{f}H$ (i.e., $u\bar{u}H$, $d\bar{d}H$, $c\bar{c}H$, $b\bar{b}H$), which are summarized in the Table 5.3. Again, I present two sepa-

Processes	σ_{Tree} (pb)	$\sigma_{\mathcal{O}_\alpha}$ (pb)	δ_{Total}%	σ_{ISR} (pb)	δ_{ISR}%
$u\bar{u}H$	3.586(3)E-02	2.948(4)E-02	-1.80E+01	3.221(2)E-02	-1.02E+01
$d\bar{d}H$	4.600(5)E-02	3.970(6)E-02	-1.37E+01	4.132(2)E-02	-1.02E+01
$c\bar{c}H$	3.580(3)E-02	2.940(4)E-02	-1.78E+01	3.215(2)E-02	-1.02E+01
$b\bar{b}H$	4.550(5)E-02	3.974(6)E-02	-1.27E+01	4.093(2)E-02	-1.01E+01

TABLE 5.3: Quark processes with the ILC proposed beam polarization at $\sqrt{s} = 250$ GeV and without experimental cuts.

rate figures for the cross-sections and total ratios. Fig. 5.3 shows the cross-sections at the tree level, as well as the $\sigma_{\mathcal{O}_\alpha}$, and ISR cross-sections. Fig 5.4 shows δ_{Total} and δ_{ISR} of the four quark processes. δ_{ISR} is approximately

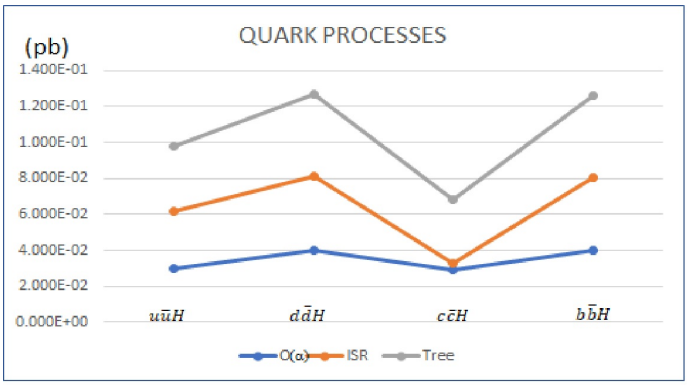

FIGURE 5.3: Cross-sections of the quark processes with the ILC proposed beam polarization at $\sqrt{s} = 250$ GeV and without experimental cuts.

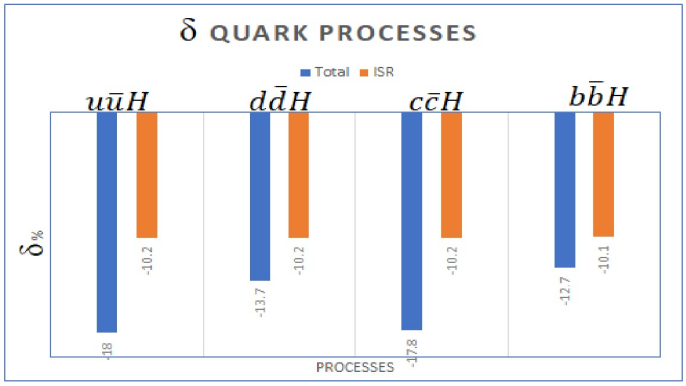

FIGURE 5.4: Ratios of the quark processes with the ILC proposed beam polarization at $\sqrt{s} = 250$ GeV and without experimental cuts.

10% for all processes. δ_{Total} of the up-type quarks is -18%, while δ_{Total} of the down-type quarks is -13% because of the charge difference or up/down

type with different iso-spins. $\sigma_{\mathcal{O}_\alpha ILCu\bar{u}H} = 2.948(4) \times 10^{-2}$ pb is larger than $\sigma_{\mathcal{O}_\alpha ILCc\bar{c}H} = 2.940(4) \times 10^{-2}$ pb as expected. These exhibit the opposite tendency to leptons. $\delta_{Total d\bar{d}H} = -13.7\%$ and $\delta_{Total b\bar{b}H} = -12.7$, with the 1% difference arising because of the Yukawa coupling. Weak corrections for the up-type and down-type quarks are approximately -8% and 3%, respectively.

Next, I compare the lepton and quark channels. For leptons, δ_{ISR} for s-channel and t-channel processes is proximately 10% and 18%, respectively; for quarks, δ_{ISR} is approximately 10% for all the cases with the ILC polarized beams and without experimental cuts. Comparing the lepton and quark channels, the difference between the up-type and the down-type are clearly observed in quarks; however, this is not observed for lepton.

I also calculated the recoil mass distribution after applying three experimental cuts for the $e^+e^- \to \mu^+\mu^- H$ process at the $\mathcal{O}(\alpha)$ corrections and including the ISR effects. The following results were obtained: $\delta_{Total} = -16.90\%$ and $\delta_{ISR} = -13.77\%$, such that the weak correction was estimated to be -3%. Thus, to measure the g_{HZZ} coupling within 1% accuracy, the weak correction of -3% cannot be neglected.

The bottom quark-Yukawa coupling was retained for the $e^+e^- \to b\bar{b}H$ process. Originally the GRACE-Loop system could produce the codes of the polarized $\mathcal{O}(\alpha)$ corrections. However, there was no function to generate such common codes to treat the collisions with various beam polarization conditions. I contributed making the new routine for treating the beam polarization for the GRACE-Loop system by adding two more variables for phase space integration.

Appendix A

The input parameters

m_u	58.0×10^{-3} GeV	m_Z	91.1876 GeV
m_d	58.0×10^{-3} GeV	m_W	80.379 GeV
m_c	1.5 GeV	m_H	125.1 GeV
m_s	92.0×10^{-3} GeV	α	1/137.035999084
m_b	4.7 GeV	$\sin^2\theta_W$	$1 - \frac{m_W^2}{m_Z^2}$
m_t	172.9 GeV	Γ_Z	2.49 GeV

TABLE A.1: Parameters

Appendix B

Electroweak theory and the on-shell renormalizaton scheme

B.1 Electroweak theory

The basic theory in this ILC energy region is the unified theory of electromagnetic and weak interactions discovered by Glashow, Weinberg and Salam about sity years ago. Here I will summarize the electroweak theoty in the Standard model. Because I do not treat QCD corrections in this thesis, then I do not mention about QCD. Later of the discovery of the electroweak theory, one of the most remarkable features of the theory, renormalizability, has been proved by 'tHooft thanks to which we are able to make the theory finite order by order of pertubation by introducing finite number of counterterms consistently.

Since then many authors have proposed various kinds of renormalization schemes suitable for higher order calculations of reactions observed in high energy colliding beam experiments. The difference among them comes from, roughly speaking, different choices in

1. physical observables by which constant parameters in the theory are to be fixed,

2. definition of wave function renormalization constants.

The most fundamental constants in the Lagrangian of the electroweak theory are $g, g^{'}, \langle\phi\rangle$, that is, two coupling constants of $SU(2)$ and $U(1)$ gauge interactions and the vacuum expectation value of the neutral Higgs scalar to make spontaneously symmetry breaking. These three parameters or their equivalents, namely, the *minimal parameters* of the theory. For the moment the fermion and purely Higgs sectors are postpone and I restrict myself to the gauge boson sector which is the key ingredient of the theory with symmetry breaking.

The mass dimension is carried solely by $\langle\phi\rangle$, which gives rise to heavy boson masses, m_Z and m_W, through Higgs-gauge field interaction, which are

they are given by

$$\begin{aligned} m_Z^2 &= \frac{1}{4}(g^2 + g'^2)\langle\phi\rangle^2, \\ m_W^2 &= \frac{1}{4}g^2\langle\phi\rangle^2, intheclassicalleve. \end{aligned} \tag{B.1}$$

from which we have

$$\frac{m_W}{m_Z} = \frac{g}{\sqrt{g^2 + g'^2}}. \tag{B.2}$$

Since the theory defines the electric charge as

$$e = \frac{gg'}{\sqrt{g^2 + g'^2}}, \tag{B.3}$$

it is clear that the theory can also be fixed by the parameters e, m_W, m_Z instead of $g, g', \langle\phi\rangle$. This choice of the minimal parameters would be the most natural one provided that we can measure m_Z and m_W by their direct productions in colliding experiments. Thus the theory is defined by physically observable quantities.

Historically other choices of minimal parameters have been used. Since the production of heavy bosons requires very high energies $\sqrt{s} > m_Z$, it has been difficult to know precise values of masses. People have been rendered to use observables available at low energies, that is

$$e, R_\nu, \Gamma_\mu(\mu \to e\bar{\nu}_e\nu_\mu), \tag{B.4}$$

where R_ν is the ratio of cross-sections for charged- and neutral-current processes induced by ν_μ-nucleon or ν_μ-e interactions and Γ_μ is the decay width of $\mu^\pm$. Among them, the electric charge e is already known as the fine structure constant, $\alpha = e^2/(4\pi)$. On the other hand, to express R_ν, the weak mixing angle, $\sin^2\theta_W$, has been used. Then R_ν is given by a function of $\sin\theta_W$, if fermion masses and the square of momentum transfer, q^2, are neglected, as being much smaller than compared with gauge boson masses,

$$R_\nu = f(\sin\theta_W), \tag{B.5}$$

by dimensional argument. In a similar way the muon decay width can be written as

$$\Gamma_\mu = m_W \cdot g(\alpha, \sin^2\theta_W). \tag{B.6}$$

By measuring R_ν, one can determine $\sin^2\theta_W$, which gives m_W because we know Γ_μ precisely. Thus all three parameters can be determined by lower energy experiments without recourse to producing heavy bosons. This is of course oversimplified as Higgs mass m_H or heavy top quark m_t being neglected. In reality the experimental data have been carefully analyzed and

compared with precise calculation up to one-loop order to deduce reliable numerical values for parameters. This is because $\sin^2\theta_W$ is rather an artificial parameter than a physical observable. When one is going to use this variable as one of minimal parameters, one should give its specified definitionof $\sin^2\theta_W$. Once we fix parameters as e, m_W, and m_Z, we have no room for the mixing angle; it will not play a primary role in the theory. All the renormalized Green's functions and thus physical quantities such as S-matrix elements and decay widths are expressed by these parameters entirely. Nevertheless we may define $\sin^2\theta_W$ as an auxiliary constant through

$$\sin^2\theta_W = 1 - \frac{m_W^2}{m_Z^2}. \tag{B.7}$$

Since $W^\pm$ and Z^0 bosons were achieved in the collider experiments, the most convenient choice of parameters is undoubtedly the set of e, m_W, and m_Z. Therefore,in the following, I will use this scheme to renormalize the theory throughout this article and I call it *canonical scheme*. The muon decay width, Eq. (B.6) is again relied on. In the canonical scheme it is expressed in another form.

$$\Gamma_\mu = m_W \cdot \tilde{g}(\alpha, m_W^2/m_Z^2), \tag{B.8}$$

and it determines m_W implicitly with possible dependence on m_H and m_t for given m_Z. Solving this equation and using the experimental value for Γ_μ, we can get m_W as a function of other parameters,

$$m_W = m_Z \cdot h(\alpha, \Gamma_\mu/m_Z). \tag{B.9}$$

Actually a scheme has been proposed which essentially takes

$$e, \Gamma_\mu, m_Z, \tag{B.10}$$

as the minimal parameters of the theory.

The second point is concerned with the stage at which one introduces wave function renormalization constants or rescaling factors for fields. If one renormalizes the wave function *before* the symmertry broken, one has the relations for gauge boson and fermions sectors,

$$\begin{aligned} A^a_{\mu 0} &= Z_W^{1/2} A^a_\mu, \\ B_{\mu 0} &= Z_B^{1/2} B_\mu, \\ \psi_{L0} &= Z_L^{1/2} \psi_L, \\ \psi^{(I)}_{R0} &= Z_R^{(I)1/2} \psi^{(I)}_R, \\ \psi^{(i)}_{R0} &= Z_R^{(i)1/2} \psi^{(i)}_R \end{aligned} \tag{B.11}$$

with

$$\psi_L = \begin{pmatrix} \psi_L^{(I)} \\ \psi_L^{(i)} \end{pmatrix}, \tag{B.12}$$

where all the fields appearing on the right-hand side are renormalized and those with subscript 0 on the left-hand side are in bared. The fields A^a_μ, $(a = 1,2,3)$ correspond to the original $SU(2)$ gauge symmetry and B_μ to $U(1)$. The left-handed fermion doublet and its upper and lower components are designated by the subscript (L) and superscripts (I) and (i), respectively. Thus there are five constants $Z_W, Z_B, Z_L, Z_R^{(I)}$ and $Z_R^{(i)}$.

On the other hand, *after* the symmertry is broken, one has to introduce more renormalization constants corresponding to the fields of physical particles; denoting photon and Z^0 fields as A_μ and Z_μ, we have

$$\begin{aligned} W^\pm_{\mu 0} &= Z_W^{1/2} W^\pm_\mu, \\ \begin{pmatrix} A^0_\mu \\ Z^0_\mu \end{pmatrix} &= \begin{pmatrix} Z_{AA}^{1/2} & Z_{AZ}^{1/2} \\ Z_{ZA}^{1/2} & Z_{ZZ}^{1/2} \end{pmatrix} \begin{pmatrix} A_\mu \\ Z_\mu \end{pmatrix}, \\ \psi^{(I)}_{L0} &= Z_L^{(I)1/2} \psi^{(I)}_L, \\ \psi^{(i)}_{L0} &= Z_L^{(i)1/2} \psi^{(i)}_L, \\ \psi^{(I)}_{R0} &= Z_R^{(I)1/2} \psi^{(I)}_R, \\ \psi^{(i)}_{R0} &= Z_R^{(i)1/2} \psi^{(i)}_R, \end{aligned} \tag{B.13}$$

i.e., nine parameters in all should be determined. Note that photon and Z^0 fields can mix with each other in the course of rescaling and that upper and lower left-handed fermions fields should be renormalized separately.

In accordance with these definitions of field rescaling, the renormalization of coupling constants is performed in different ways depending on the schemes. In the gauge symmertric scheme, it is natural to introduce the counterterms for two original gauge coupling constants and Higgs vacuum expectation value $v_0 = \langle \phi_0 \rangle$ and to renormalize them by

$$\begin{aligned} g_0 &= g + \delta g, \\ g'_0 &= g' + \delta g', \\ v_0 &= v + \delta v, \end{aligned} \tag{B.14}$$

to respect the symmetry as far as possible. In the canonical scheme the renormalized parameters g, g', and v should be fixed by the observables e, m_Z, and m_W or their equivalents. Therefore we have to give three relations which connect two sets of renormalized parameters,

$$\begin{aligned} g &= f_1(e, m_Z, m_W), \\ g' &= f_2(e, m_Z, m_W), \\ v &= f_3(e, m_Z, m_W). \end{aligned} \tag{B.15}$$

The merit of the symmetric scheme is that the original gauge symmetries are manifest in renormalization constants and thus the counterterms generated by Eqs. (B.11) and (B.14) are simple thanks to the fact that the minimal number of them are introduced. The demerit would be that the way to connect them with observables are somewhat obscure and complicated. Different from the ordinary way of renormalization, the renormalized fields are defined before symmertry breaking and thus they themselves do not correspond to any physical particles except $W^{\pm}$ boson. Thus the on-shell conditions cannot be applied to gauge bosons and fermion doublets in a direct way. As long as the theory is fixed only by three parameters g, $g^{'}$, and v the relations eqs are uniquely determined. This is, however, not the only way to relate the renormalized parameters g, $g^{'}$, and v in *one* scheme to those in *another* scheme. It is possible to give relations different from Eq. (B.15) by introducing a redundant parameter ρ, which requires a further renormalization condition or a constrained equation. In fact it is this type of redundancy which often leads to the confusion in the definition of the weak mixing angle $\sin^2\theta_W$.

On the other hand, when the symmetry is broken before the renormalization, one must re-express all the constants in the Lagrangian by the bare e, m_{Z0}, and m_{W0}. Renormalization is done on these parameters,

$$\begin{aligned} e_0 &= e + \delta e, \\ m_{Z0}^2 &= m_Z^2 + \delta m_Z^2, \\ m_{W0}^2 &= m_W^2 + \delta m_W^2. \end{aligned} \tag{B.16}$$

In the on-shell scheme, the renormalization constants show no trace of the original gauge symmetries either in rescaling of fields or in renormalizing constant parameters. However, since all physical particles are treated independently, the on-shell renormalization condition can be applied in a straightforward way. Further the parameters of the theory are fixed unambiguously by observables e, m_Z, and m_W. I can say this is the principal merit of this scheme. The coupling constants attached at the vertices, however, have complicated forms when they are rewritten in terms of these basic parameters, which in turn gives rise to lengthy counterterms. Needless to say, any two schemes should give the same physical results provided that they are constructed in a self-consistent way.

B.2 Lagrangian

The electroweak Lagrangian is composed of two parts; the first part has the same form as the classical Lagrangian, containing physical objects and the second one is related to the subsidiary conditions to fix the ambiguity of gauge freedom,

$$\mathcal{L} = \mathcal{L}_{cl} + \mathcal{L}_{\text{gauge fix.}} \tag{B.17}$$

In this section, I present the derivation of renormalized Lagrangian from the original gauge symmetric, unrenormalized one. Since I follow the scheme of [13], I simply review and reproduce the results obtained with brief explanations. All the complicated theoretical arguments such as renormalizability, BRS tranformation, Slavnov-Taylor identity or gauge fixing procedure, etc., are omitted; they are left to other literatures, for example, to [13].

In the first half of this section I present $\mathcal{L}_{cl}$. In order to stress tha we have only unrenormalized fields and constants at the beginning, I put the subscript 0 to all of them. The renormalized quantities appearing later are denoted by the same ones without 0. Decomposing the Lagrangian $\mathcal{L}_{cl}$ into several parts, I write them as

$$\mathcal{L}_{cl} = \mathcal{L}_G + \mathcal{L}_F + \mathcal{L}_H + \mathcal{L}_M, \tag{B.18}$$

where $\mathcal{L}_G$ is the gauge boson part, $\mathcal{L}_F$ is the fermion kinetic part, $\mathcal{L}_H$ is the Higgs scalar part and $\mathcal{L}_M$ is the fermion- Higgs interaction. The pure gauge boson part is expressed by the field strengths of $SU(2)$ and $U(1)$ gauge fields,

$$\mathcal{L}_G = -\frac{1}{4} G^a_{\mu\nu 0} G^a_{\mu\nu 0} - \frac{1}{4} F_{\mu\nu 0} F_{\mu\nu 0}, \tag{B.19}$$

where

$$\begin{aligned} G^a_{\mu\nu 0} &= \partial_\mu A^a_{\nu 0} - \partial_\nu A^a_{\mu 0} + g_0 \epsilon_{abc} A^b_{\mu 0} A^c_{\nu 0}, \\ F_{\mu\nu 0} &= \partial_\mu B_{\nu 0} - \partial_\nu B_{\mu 0}, \end{aligned} \tag{B.20}$$

are field strengths for gauge fields $A^a_{\mu 0} (a = 1, 2, 3)$, and $B_{\mu 0}$, respectively; and the repeated indices imply the sum over a, b or c. The kinetic part of fermions, both quarks and leptons, including gauge interactions is given by

$$\mathcal{L}_F = \sum_L \bar{\psi}_{L0} (i \not{\partial} + g_0 T_a A^a_{\mu 0}) \psi_{L0} + \sum_{f=i,I} \bar{\psi}^{(f)}_{R0} (i \not{\partial} + g^{'}_0 B^a_{\mu 0}) \psi^{(f)}_{R0}, \tag{B.21}$$

where ψ_{L0} and ψ_{R0} represent $SU(2)$ doublet and singlet fermion fields, respectively, with

$$\psi_{L0} = \begin{pmatrix} \psi^{(I)}_{L0} \\ \psi^{(i)}_{L0} \end{pmatrix}, \tag{B.22}$$

and the sum of left-handed fermions is taken over all doublets. Throughout this article, the subscript (L), and the superscripts (I), (i), and (f) stand for left-handed fermion doublet and upper, lower and all kinds of fermions, respectively. The coupling constant g_0 corresponds to $SU(2)$ and $g^{'}_0$ to $U(1)$ gauge interactions and the T_a's are related to $SU(2)$ Pauli matrices,

$$T_a = \frac{\tau_a}{2}. \qquad (a = 1, 2, 3) \tag{B.23}$$

The Higgs scalar part with gauge interaction is

$$\mathcal{L}_H = \left| \left(\partial_\mu - i g_0 T_a A^a_{\mu 0} - i \frac{g_0^{'}}{2} B_{\mu 0} \right) \Phi_0 \right|^2 + \mu_0^2 \Phi_0^\dagger \Phi_0 - \lambda_0 (\Phi_0^\dagger \Phi_0)^2, \tag{B.24}$$

and the fermion-Higgs interactions are written in the form,

$$\mathcal{L}_M = -\sum_i f_0^{(i)} \bar{\Psi}^{(i)}_{L0} \Phi_0 \psi^{(i)}_{R0} - \sum_I f_0^{(I)} \bar{\Psi}^{(I)}_{L0} (i\tau_2 \Phi_0^\dagger) \psi^{(I)}_{R0} + h.c., \tag{B.25}$$

where $f_0^{(i)}$ and $f_0^{(I)}$ are Yukawa couplings which generate fermion masses through the symmetry breaking. Two new combinations of fields, $\Psi^{(i)}_{L0}$ and $\Psi^{(I)}_{L0}$, for left-handed fermions are introduced so as to make the mass matrix diagonal from the outset,

$$\Psi^{(i)}_{L0} = \begin{pmatrix} \sum_I U_{iI} \psi^{(I)}_{L0} \\ \psi^{(i)}_{L0} \end{pmatrix},$$

$$\Psi^{(I)}_{L0} = \begin{pmatrix} \psi^{(I)}_{L0} \\ \sum_I U^{-1}_{iI} \psi^{(i)}_{L0} \end{pmatrix}, \tag{B.26}$$

$$\tag{B.27}$$

where U_{iI} is the Kobayashi-Maskawa mixing matrix for quarks.

Next task is to break the symmetries by introducing the vacuum expectation value of the Higgs field Φ_0. It is achieved by putting in the form,

$$\Phi_0 = \begin{pmatrix} i\chi_0^+ \\ \frac{v_0 + \phi_0 - i\chi_{30}}{\sqrt{2}} \end{pmatrix}, \tag{B.28}$$

where v_0 is the bare vacuum expectation value, ϕ_0 is the physical Higgs scalar field, χ_{30} is the neutral Goldstone boson, and χ^+ is the charged Goldstone boson

$$\chi_0^\pm = \frac{1}{\sqrt{2}} (\chi_{10} \mp i\chi_{20}). \tag{B.29}$$

Substituting this into the Lagrangian and redefining new fields for physical gauge bosons,

$$\begin{aligned} W^\pm_{\mu 0} &= \frac{1}{\sqrt{2}} (A^1_{\mu 0} \mp i A_{\mu 0}), \\ Z_{\mu 0} &= \frac{1}{\sqrt{g_0^2 + g_0^{'2}}} (g_0 A^3_{\mu 0} - g_0^{'} B_{\mu 0}), \\ A_{\mu 0} &= \frac{1}{\sqrt{g_0^2 + g_0^{'2}}} (g_0^{'} A^3_{\mu 0} + g_0 B_{\mu 0}), \end{aligned} \tag{B.30}$$

I get unrenormalized Lagrangian for physical particles. The bosonic part then becomes

$$\begin{aligned}
\mathcal{L}_G = \quad & -\frac{1}{2}\left|\partial_\mu W^+_{\nu 0} - \partial_\nu W^+_{\mu 0}\right|^2 - \frac{1}{4}(\partial_\mu Z_{\nu 0} - \partial_\nu Z_{\mu 0})^2 - \frac{1}{4}(\partial_\mu A_{\nu 0} - \partial_\nu A_{\mu 0})^2 \\
& + \frac{i g_0}{\sqrt{g_0^2 + g_0^{\prime 2}}}(g_{\alpha\gamma}g_{\beta\delta} - g_{\alpha\delta}g_{\beta\gamma}) \\
& \Big[g_0 \Big\{ (\partial_\alpha W^+_{\beta 0}) W^-_{\gamma 0} Z_{\delta 0} + (\partial_\alpha W^-_{\beta 0}) W^+_{\delta 0} Z_{\gamma 0} + (\partial_\alpha Z_{\beta 0}) W^+_{\gamma 0} Z_{\delta 0} \Big\} \\
& + g_0^{'} \Big\{ (\partial_\alpha W^+_{\beta 0}) W^-_{\gamma 0} A_{\delta 0} + (\partial_\alpha W^-_{\beta 0}) A_{\gamma 0} W^+_{\delta 0} + (\partial_\alpha A_{\beta 0}) W^+_{\gamma 0} W^-_{\delta 0} \Big\} \Big] \\
& + \frac{g_0^2}{g_0^2 + g_0^{\prime 2}} \Big[(g_{\alpha\beta}g_{\gamma\delta} - g_{\alpha\gamma}g_{\beta\delta}) W^+_{\alpha 0} W^-_{\beta 0} (g_0^2 Z_{\gamma 0} Z_{\delta 0} + g_0^{'} A_{\gamma 0} A_{\delta 0}) \\
& + (2 g_{\alpha\beta}g_{\gamma\delta} - g_{\alpha\gamma}g_{\beta\delta} - g_{\alpha\delta}g_{\beta\gamma}) g_0 g_0^{'} W^+_{\alpha 0} W^-_{\beta 0} A_{\gamma 0} Z_{\delta 0} \Big] \\
& + (g_{\alpha\beta}g_{\gamma\delta} - g_{\alpha\gamma}g_{\beta\delta}) \frac{g_0^2}{2} W^+_{\alpha 0} W^+_{\beta 0} W^-_{\gamma 0} W^-_{\delta 0},
\end{aligned} \tag{B.31}$$

and the fermion part is

$$\begin{aligned}
\mathcal{L}_F = \quad & \sum_f i \bar{\psi}_0^{(f)} \not{\partial} \psi_0^{(f)} \\
& + \frac{g_0}{\sqrt{2}} \sum_{i,I} (\bar{\psi}_0^{(I)} U^\dagger_{iI} \gamma_\mu \frac{1-\gamma_5}{2} \psi_0^{(i)} W^+_{\mu 0} + \bar{\psi}_0^{(i)} U_{iI} \gamma_\mu \frac{1-\gamma_5}{2} \psi_0^{(I)} W^-_{\mu 0}) \\
& + e_0 \sum_f Q_f \bar{\psi}_0^{(f)} \gamma_\mu \psi_0^{(f)} A_{\mu 0} \\
& \frac{\sqrt{g_0^2 + g_0^{\prime 2}}}{2} \sum_f \bar{\psi}_0^{(f)} \gamma_\mu \Big[T_{3f}(1-\gamma_5) - 2 Q_f \frac{g_0^{\prime 2}}{g_0^2 + g_0^{\prime 2}} \Big] \psi_0^{(f)} Z_{\mu 0},
\end{aligned} \tag{B.32}$$

where the ψ without L or R is the Dirac spinor by which I define

$$\psi_L = \frac{1-\gamma_5}{2}\psi, \qquad \psi_R = \frac{1+\gamma_5}{2}\psi \tag{B.33}$$

namely, $\psi = \psi_L + \psi_R$. Further we have introduced the bare electric charge by

$$e_0 = \frac{g_0 g_0^{'}}{\sqrt{g_0^2 + g_0^{\prime 2}}} \tag{B.34}$$

to stress the fermion-photon interaction and Q_f is the charge of f-th fermion in units of e_0. Since the Higgs scalar part is very complicated and develops too many terms, we divide it further into four parts,

$$\mathcal{L}_H = \mathcal{L}_H^{(2)} + \mathcal{L}_H^{(3)} + \mathcal{L}_H^{(4)} + \mathcal{L}_V. \tag{B.35}$$

The first part contains kinetic terms for scalar particles and bilinear terms in fields,

$$\begin{aligned}\mathcal{L}_H^{(2)} = \quad & +\frac{1}{2}(\partial_\mu \phi_0)^2 + \frac{1}{2}(\partial_\mu \chi_{30})^2 + (\partial_\mu \chi_0^+)(\partial_\mu \chi_0^-) \\ & + m_{W0}^2 W_{\mu 0}^+ W_{\mu 0}^- + \frac{1}{2} m_{Z0}^2 Z_{\mu 0} Z_{\mu 0} \\ & - \frac{1}{2} g_0 v_0 [W_{\mu 0}^+ (\partial_\mu \chi_0^-) + W_{\mu 0}^- (\partial_\mu \chi_0^+)] - \frac{1}{2}\sqrt{g_0^2 + g_0'^2}\, v_0 Z_{\mu 0} (\partial_\mu \chi_{30}),\end{aligned} \tag{B.36}$$

where the bare mass terms of gauge bosons have been rewritten by using the bare relations,

$$\begin{aligned} m_{Z0}^2 &= \frac{1}{4}(g_0^2 + g_0'^2) v_0^2, \\ m_{W0}^2 &= \frac{1}{4} g_0^2 v_0^2. \end{aligned} \tag{B.37}$$

The cubic and quartic parts in fields contain interaction terms between Higgs and gauge fields,

$$\begin{aligned}\mathcal{L}_H^{(3)} = \quad & \frac{1}{2} g_0 W_{\mu 0}^+ (\chi_0^- \overleftrightarrow{\partial}_\mu \phi_0) + \frac{1}{2} g_0 W_{\mu 0}^- (\chi_0^+ \overleftrightarrow{\partial}_\mu \phi_0) \\ & + \frac{i}{2} g_0 W_{\mu 0}^+ (\chi_{30} \overleftrightarrow{\partial}_\mu \chi_0^-) - \frac{i}{2} g_0 W_{\mu 0}^- (\chi_{30} \overleftrightarrow{\partial}_\mu \chi_0^+) \\ & + \frac{1}{2}\sqrt{g_0^2 + g_0'^2}\, Z_{\mu 0} (\chi_{30} \overleftrightarrow{\partial}_\mu \phi_0) \\ & + \frac{i}{2} \frac{g_0^2 - g_0'^2}{\sqrt{g_0^2 + g_0'^2}} Z_{\mu 0} (\chi_0^- \overleftrightarrow{\partial}_\mu \chi_0^+) \\ & + \frac{i g_0 g_0'}{\sqrt{g_0^2 + g_0'^2}} A_{\mu 0} (\chi_0^- \overleftrightarrow{\partial}_\mu \chi_0^+),\end{aligned} \tag{B.38}$$

$$
\begin{aligned}
\mathcal{L}_H^{(4)} = \quad & \frac{1}{4}g_0^2 W_{\mu 0}^+ W_{\mu 0}^- (2v_0\phi_0 + \phi_0^2 + 2\chi_0^+\chi_0^- + \chi_{30}^2) \\
& + \frac{1}{4}\frac{(g_0^2 - g_0'^2)^2}{g_0^2 + g_0'^2} Z_{\mu 0} Z_{\mu 0} (\chi_0^-\chi_0^+) + \frac{1}{8}(g_0^2 + g_0'^2) Z_{\mu 0} Z_{\mu 0} (2v_0\phi_0 + \phi_0^2 + \chi_{30}^2) \\
& + \frac{g_0^2 g_0'^2}{g_0^2 + g_0'^2} A_{\mu 0} A_{\mu 0} (\chi_0^+\chi_0^-) + \frac{g_0 g_0' (g_0^2 - g_0'^2)}{g_0^2 + g_0'^2} A_{\mu 0} Z_{\mu 0} (\chi_0^+\chi_0^-) \\
& + \frac{1}{2}\frac{g_0 g_0'^2}{\sqrt{g_0^2 + g_0'^2}} (Z_{\mu 0} W_{\mu 0}^+ \chi_0^-)(\chi_{30} + iv_0 + i\phi_0) \\
& + \frac{1}{2}\frac{g_0 g_0'^2}{\sqrt{g_0^2 + g_0'^2}} (Z_{\mu 0} W_{\mu 0}^- \chi_0^+)(\chi_{30} - iv_0 - i\phi_0) \\
& - \frac{1}{2}\frac{g_0^2 g_0'}{\sqrt{g_0^2 + g_0'^2}} (A_{\mu 0} W_{\mu 0}^+ \chi_0^-)(\chi_{30} + iv_0 + i\phi_0) \\
& - \frac{1}{2}\frac{g_0^2 g_0'}{\sqrt{g_0^2 + g_0'^2}} (A_{\mu 0} W_{\mu 0}^- \chi_0^+)(\chi_{30} - iv_0 - i\phi_0)
\end{aligned}
\tag{B.39}
$$

The last part is the *potential* term for Higgs particle,

$$
\begin{aligned}
\mathcal{L}_V = \quad & T_0\phi_0 + (\mu_0^2 - \lambda_0 v_0^2)\chi_0^+\chi_0^- \\
& + \frac{1}{2}(\mu_0^2 - \lambda_0 v_0^2)\chi_{30}^2 + \frac{1}{2}(\mu_0^2 - 3\lambda_0 v_0^2)\phi_0^2 \\
& - 2v_0\lambda_0(\phi_0\chi_0^+\chi_0^-) - v_0\lambda_0(\phi_0\chi_{30}\chi_{30}) - v_0\lambda_0\phi_0^3 \\
& - \lambda_0(\chi_0^+\chi_0^-)^2 - \lambda_0(\chi_0^+\chi_0^-)\chi_{30}^2 - \lambda_0(\chi_0^+\chi_0^-)\phi_0^2 \\
& - \frac{1}{4}\lambda_0\chi_{30}^4 - \frac{1}{4}\lambda_0\phi_0^4 - \frac{1}{2}\lambda_0\chi_{30}^2\phi_0^2,
\end{aligned}
\tag{B.40}
$$

where the coefficient of the counterterm for tadpole diagrams is re written as

$$
T_0 = v_0(\mu_0^2 - \lambda_0 v_0^2). \tag{B.41}
$$

The fermion mass part yields

$$
\begin{aligned}
\mathcal{L}_M = \quad & -\sum_f m_{f0}\bar{\psi}_0^{(f)}\psi_0^{(f)} \\
& - \frac{i}{2}\sum_{i,I} \bar{\psi}_0^{(I)} U_{Ii}^\dagger \Big[(f_0^{(i)} - f_0^{(I)}) + (f_0^{(i)} + f_0^{(I)})\gamma_5 \Big] \psi_0^{(i)}\chi_0^+ \\
& - \frac{i}{2}\sum_{i,I} \bar{\psi}_0^{(i)} U_{Ii} \Big[(f_0^{(I)} - f_0^{(i)}) + (f_0^{(i)} + f_0^{(I))})\gamma_5 \Big] \psi_0^{(I)}\chi_0^- \\
& - \sum_i \frac{f_0^{(f)}}{\sqrt{2}}\phi_0\bar{\psi}_0^{(f)}\psi_0^{(f)} + \sum_f \frac{if_0^{(i)}}{\sqrt{2}}\chi_{30}\bar{\psi}_0^{(i)}\gamma_5\psi_0^{(i)} - \sum_I \frac{if_0^{(I)}}{\sqrt{2}}\chi_{30}\bar{\psi}_0^{(I)}\gamma_5\psi_0^{(I)}.
\end{aligned}
\tag{B.42}
$$

According to our choice of minimal parameters, we rewrite all the bare constants, $g_0, g_0^{'}$, and v_0 by bare parameters, e_0, m_{Z0}, and m_{W0}, in the following way:

$$\begin{aligned}
g_0 &= e_0 \frac{m_{Z0}}{\sqrt{m_{Z0}^2 - m_{W0}^2}}, \qquad g_0^{'} = e_0 \frac{m_{Z0}}{m_{W0}}, \\
v_0 &= \frac{2}{e_0} \frac{m_{W0}}{m_{Z0}} \sqrt{m_{Z0}^2 - m_{W0}^2}, \\
\lambda_0 &= \frac{e_0^2 m_{Z0}^2}{8 m_{W0}^2 (m_{Z0}^2 - m_{W0}^2)} (m_{H0}^2 - \frac{e_0 T_0 m_{Z0}}{m_{W0} \sqrt{m_{Z0}^2 - m_{W0}^2}}), \\
\mu_0^2 &= m_{H0}^2/2, \\
f_0^{(f)} &= \sqrt{2} m_{f0}/v_0.
\end{aligned} \tag{B.43}$$

By these replacements, we can get the final form of the bare Lagrangian by which we have to describe all physical phenomena.

The next step is to renormalize the bare Lagrangian. It consists of two procedures; one is redefinition of the constants and the other is rescaling of particle fields. The first one is to express the bare constants by a sum of finite renormalized quantities and their counterterms,

$$\begin{aligned}
m_{W0}^2 &= m_W^2 + \delta m_W^2, \\
m_{Z0}^2 &= m_Z^2 + \delta m_Z^2, \\
m_{H0}^2 &= m_H^2 + \delta m_H^2, \\
m_{f0}^2 &= m_f + \delta m_f, \\
e_0 &= Ye.
\end{aligned} \tag{B.44}$$

The rescalings of gauge fields $(Z^0, W^{\pm}, \gamma)$ are defined by

$$\begin{aligned}
W_{\mu 0}^{\pm} &= Z_W^{1/2} W_{\mu}^{\pm}, \\
\begin{pmatrix} A_{\mu}^0 \\ Z_{\mu}^0 \end{pmatrix} &= \begin{pmatrix} Z_{AA}^{1/2} & Z_{AZ}^{1/2} \\ Z_{ZA}^{1/2} & Z_{ZZ}^{1/2} \end{pmatrix} \begin{pmatrix} A_{\mu} \\ Z_{\mu} \end{pmatrix},
\end{aligned} \tag{B.45}$$

and those for left- and right-handed fermions are

$$\begin{aligned}
\psi_{L0}^{(I)} &= Z_L^{(I)1/2} \psi_L^{(I)}, \\
\psi_{L0}^{(i)} &= Z_L^{(i)1/2} \psi_L^{(i)}, \\
\psi_{R0}^{(I)} &= Z_R^{(I)1/2} \psi_R^{(I)}, \\
\psi_{R0}^{(i)} &= Z_R^{(i)1/2} \psi_R^{(i)}.
\end{aligned} \tag{B.46}$$

In the presence of quark mixing, Z_L and Z_R become matrices which connect bare and renormalized fermion fields of the *same charge*:

$$\begin{aligned}\psi^{(f)}_{R,L0} &= \sum_{f'} (Z^{1/2}_{R,L})_{f,f'} \psi^{(f')}_{R,L}, \\ \bar{\psi}^{(f)}_{R,L0} &= \sum_{f'} \bar{\psi}^{(f')}_{R,L} (Z^{1/2\dagger}_{R,L})_{f',f}.\end{aligned} \tag{B.47}$$

The Higgs boson is rescaled as

$$\phi_0 = Z^{1/2}_{\phi} \phi. \tag{B.48}$$

Now we turn to the gauge fixing part of the original Lagrangian. This contains physical particles, Goldstone bosons and ghosts, that is, the gauge fixing term and the Faddeev-Povov ghost parts,

$$\mathcal{L}_{\text{gauge fix.}} = \mathcal{L}_{GF} + \mathcal{L}_{FP} \tag{B.49}$$

The gauge fixing term is written in the renormalized form,

$$\begin{aligned}\mathcal{L}_{GF} = \quad & -\frac{1}{\alpha_W} (\partial_\mu W^+_\mu + \alpha_W m_W \chi^+) \cdot (\partial_\mu W^-_\mu + \alpha_W m_W \chi^-) \\ & -\frac{1}{2\alpha_Z} (\partial_\mu Z_\mu + \alpha_Z m_Z \chi_3)^2 - \frac{1}{2\alpha_A} (\partial_\mu A_\mu)^2.\end{aligned} \tag{B.50}$$

Renormalzation of bare gauge paraneters, α_{W0}, α_{Z0}, and α_{A0}, and rescalings of Goldstone boson fields $\chi^{\pm}_0$, χ_{30} are follows: Those for gauge parameters are given by

$$\begin{aligned}\alpha_{W0} &= \alpha_W Z^{1/2}_W Z^{-1/2}_{\chi} / \sqrt{1 + \delta m^2_W / m^2_W}, \\ \alpha_{Z0} &= \alpha_Z Z^{1/2}_{ZZ} Z^{-1/2}_{\chi^3} / \sqrt{1 + \delta m^2_Z / m^2_Z}, \\ \beta_{Z0} &= \alpha_Z Z^{1/2}_{AZ} Z^{-1/2}_{\chi^3} / \sqrt{1 + \delta m^2_Z / m^2_Z},\end{aligned} \tag{B.51}$$

and field rescaling are by

$$\begin{aligned}\chi^{\pm}_0 &= Z^{1/2}_{\chi} \chi^{\pm}, \\ \chi_{30} &= Z^{1/2}_{\chi_3} \chi_3.\end{aligned} \tag{B.52}$$

A few words should be given on the choice of numerical values for these parameters: They Feynman gauge, which has often been used in literature, is defined by

$$\alpha_W = \alpha_Z = \alpha_A = 1, \tag{B.53}$$

while the unitary gauge is chosen by letting all these parameters infinity. When one calculates loop diagrams, the former gauge is convenient because the gauge boson propagators take the simplest forms without longitudinal

parts. However, one has to include all possible diagrams which contain unphysical particles, i.e., Goldstone bosons and ghosts. Thus there are a lot of diagrams to be considered. On the other hand, the Lagrangian with unitary gauge has no such unphysical particles at all. The number of diagrams is, thus, much less than the former. The propagators of gauge bosons, however, develop longitudinal parts, which cause much complications in the calculations, because of the appearance of the double-pole like term. Decomposing this into a sum of single-pole term, we have a lenghty expression for general gauge parameters. Generally speaking, the 'tHooft-Feynman gauge is convenient in higher order calculations. Needless to say, the final answers should be independent of the choice of gauge parameters.

The last part of the Lagrangian os the Faddeev-Povov ghost part. In accordance with the gauge fixing term, it is given by

$$\begin{aligned}\mathcal{L}_{FP} = &-\bar{c}_0^+ \delta_{BRS}(\partial_\mu W_{\mu 0}^- + \alpha_{W0} m_{W0} \chi_0^-) - \bar{c}_0^- \delta_{BRS}(\partial_\mu W_{\mu 0}^+ + \alpha_{W0} m_{Z0} \chi_0^+) \\ &-\bar{c}_0^Z \delta_{BRS}(\partial_\mu Z_{\mu 0} + \alpha_{Z0} m_{Z0} \chi_{30}) - \bar{c}_0^A \delta_{BRS}(\partial_\mu A_{\mu 0} + \beta_{Z0} m_{W0} \chi_{30}),\end{aligned} \tag{B.54}$$

where every quantity is bare and the BRS transformations for the fields are defined by

$$\begin{aligned}
\delta_{BRS} W_{\mu 0}^\pm &= \partial_\mu c_0^\mu \pm \frac{i g_0}{\sqrt{g_0^2 + g_0^{\prime 2}}} [W_{\mu 0}^\pm (g_0 c_0^Z + g_0^{'} c_0^A) - (g_0 Z_{\mu 0} + g_0^{'} A_{\mu 0}) c_0^\pm], \\
\delta_{BRS} Z_{\mu 0} &= -\frac{i g_0^2}{\sqrt{g_0^2 + g_0^{\prime 2}}} (W_{\mu 0}^+ c_0^- - W_{\mu 0}^- c_0^+) + \partial_\mu c_0^Z, \\
\delta_{BRS} A_{\mu 0} &= -\frac{i g_0 g_0^{'}}{\sqrt{g_0^2 + g_0^{\prime 2}}} (W_{\mu 0}^+ c_0^- - W_{\mu 0}^- c_0^+) + \partial_\mu c_0^A, \\
\delta_{BRS} \phi_0 &= -\frac{g_0}{2} (\chi_0^+ c_0^- + \chi_0^- c_0^+) - \frac{\sqrt{g_0^2 + g_0^{\prime 2}}}{2} \chi_{30} c_0^Z, \\
\delta_{BRS} \chi_0^\pm &= +\frac{g_0}{2} [(v_0 + \phi_0) c_0^\pm \mp \chi_{30} c_0^\pm] \pm \frac{i}{2\sqrt{g_0^2 + g_0^{\prime 2}}} \chi_0^\pm [(g_0^2 - g_0^{\prime 2}) c_0^Z + 2 g_0 g_0^{'} c^A], \\
\delta_{BRS} \chi_{30} &= \frac{\sqrt{g_0^2 + g_0^{\prime 2}}}{2} (v_0 + \phi_0) c_0^Z - \frac{i g_0}{2} (\chi_0^+ c_0^- - \chi_0^- c_0^+).
\end{aligned} \tag{B.55}$$

Here the original ghost field c_0^3, c_0^0 are replaced by

$$\begin{aligned}
c_0^Z &= \frac{1}{\sqrt{g^2 + g^{\prime 2}}} \cdot (g_0 c_0^3 - g_0^{'} c_0^0), \\
c_0^A &= \frac{1}{\sqrt{g^2 + g^{\prime 2}}} \cdot (g_0^{'} c_0^3 - g_0^c),
\end{aligned} \tag{B.56}$$

in the same way as the mixing between physical Z^0 and photon fields. Thus the Faddeev-Povov ghost part, divided into bilinear and curbic terms in fields, is given by

$$\mathcal{L}_{FP} = \mathcal{L}_{FP}^{(2)} + \mathcal{L}_{FP}^{(3)}, \tag{B.57}$$

where

$$\begin{aligned}\mathcal{L}^{(2)} = &-\bar{c}_0^+(\partial_\mu^2 + \alpha_{W0}m_{W0}^2)c_0^- - \bar{c}_0^-(\partial_\mu^2 + \alpha_{W0}m_{W0}^2)c_0^+ \\ &-\bar{c}_0^Z(\partial_\mu^2 + \alpha_{Z0}m_{Z0}^2)c_0^Z - \bar{c}_0^A\partial_\mu^2 c_0^A - \bar{c}_0^A(\beta_0 m_{W0}^2)c_0^Z\end{aligned} \tag{B.58}$$

and

$$\begin{aligned}\mathcal{L}^{(3)} = \quad & \frac{ig_0^2}{\sqrt{g_0^2+g_0'^2}}W_{\mu 0}^+[\partial_\mu\bar{c}_0^-\cdot c_0^Z - \partial_\mu\bar{c}_0^Z\cdot c_0^-] \\ &-\frac{ig_0^2}{\sqrt{g_0^2+g_0'^2}}W_{\mu 0}^-[\partial_\mu\bar{c}_0^+\cdot c_0^Z - \partial_\mu\bar{c}_0^Z\cdot c_0^+] \\ &+ie_0W_{\mu 0}^+[\partial_\mu\bar{c}_0^-\cdot c_0^A - \partial_\mu\bar{c}_0^A\cdot c_0^-] - ie_0W_{\mu 0}^-[\partial_\mu\bar{c}_0^+\cdot c_0^A - \partial_\mu\bar{c}_0^A\cdot c_0^+] \\ &+\frac{ig_0^2}{\sqrt{g_0^2+g_0'^2}}Z_{\mu 0}[\partial_\mu\bar{c}_0^+\cdot c_0^- - \partial_\mu\bar{c}_0^-\cdot c_0^+] + ie_0A_{\mu 0}^+[\partial_\mu\bar{c}_0^+\cdot c_0^- - \partial_\mu\bar{c}_0^-\cdot c_0^+] \\ &+i\chi_0^+\Big[\frac{-\alpha_{W0}m_{W0}(-g_0'^2+g_0^2)}{2\sqrt{g_0'^2+g_0^2}}\bar{c}_0^-c_0^Z - \alpha_{W0}m_{W0}e_0\bar{c}_0^-c_0^A \\ &+\frac{\beta_0}{2}m_{Z0}g_0\bar{c}_0^Ac_0^- + \frac{\alpha_{Z0}}{2}m_{Z0}g_0\bar{c}_0^Zc_0^-\Big] \\ &+i\chi_0^-\Big[\frac{+\alpha_{W0}m_{W0}(-g_0'^2+g_0^2)}{2\sqrt{g_0'^2+g_0^2}}\bar{c}_0^+c_0^Z + \alpha_{W0}m_{W0}e_0\bar{c}_0^+c_0^A \\ &-\frac{\beta_0}{2}m_{Z0}g_0\bar{c}_0^Ac_0^+ - \frac{\alpha_{Z0}}{2}m_{Z0}g_0\bar{c}_0^Zc_0^+\Big] \\ &+\frac{i\alpha_{W0}}{2}m_{W0}g_0\chi_{30}[-\bar{c}_0^+c_0^- + \bar{c}_0^-c_0^+] - \frac{\alpha_{W0}}{2}m_{W0}g_0\phi_0[-\bar{c}_0^+c_0^- + \bar{c}_0^-c_0^+] \\ &-\frac{\alpha_{Z0}}{2}m_{Z0}\sqrt{g_0'^2+g_0^2}\phi\bar{c}_0^Zc_0^Z - \frac{\beta_{Z0}}{2}m_{Z0}\sqrt{g_0'^2+g_0^2}\phi\bar{c}_0^Ac_0^Z.\end{aligned} \tag{B.59}$$

Renormalizations of gauge parameters are given in Eq. (B.51) and those for ghost fields are defined by the following equations,

$$\begin{aligned}&c_0^\pm = \tilde{Z}_3c^\pm, \\ &\begin{pmatrix} c_0^Z \\ c_0^A \end{pmatrix} = \begin{pmatrix} \tilde{Z}_{ZZ} & \tilde{Z}_{ZA} \\ \tilde{Z}_{AZ} & \tilde{Z}_{AA} \end{pmatrix}\begin{pmatrix} c^Z \\ c^A \end{pmatrix}, \\ &\bar{c}_0^\pm = \bar{c}^\pm, \quad \bar{c}_0^Z = \bar{c}^Z, \quad \bar{c}_0^A = \bar{c}^A.\end{aligned} \tag{B.60}$$

It should be noted that the ghost field c and anti-ghost $\bar{c}$ are rescaled in different ways. This is because these two fields are not connected by particle and anti-particle relation but rather independent objects.

Now we can re-expess the orriginal Lagrangian $\mathcal{L}$ by both renormalized fields and constants. It is straightforward to divide it into free and interaction parts as defined in the last paragraph of the previous section. The free Lagrangian $\mathcal{L}_{tree}$ is obtained from the bilinear terms in fields in $\mathcal{L}$ by letting all rescaling factors to be unity, $Z_i = 1$, and all mass counterterms to vanish, $\delta m_i^2 = 0$. Thus we have

$$\begin{aligned}
\mathcal{L}_{tree} = \quad & W_\mu^+ \Big[g^{\mu\nu}(\partial_\alpha^2 + m_W^2) - (1 - \frac{1}{\alpha_W}\partial_\mu\partial_\nu) \Big] W_\nu^- \\
& + \frac{1}{2} Z_\mu \Big[g^{\mu\nu}(\partial_\alpha^2 + m_Z^2) - (1 - \frac{1}{\alpha_Z}\partial_\mu\partial_\nu) \Big] Z_\nu \\
& + \frac{1}{2} A_\mu \Big[g^{\mu\nu}\partial_\alpha^2 - (1 - \frac{1}{\alpha_A}\partial_\mu\partial_\nu) \Big] A_\nu \\
& + \sum_f \bar{\psi}^{(f)}(i\,\partial\!\!\!/ - m_f)\psi^{(f)} \frac{1}{2}\phi(\partial_\alpha^2 + m_H^2)\phi \\
& - \chi^+(\partial_\alpha^2 + \alpha_W m_W^2)\chi^- - \frac{1}{2}\chi_3(\partial_\alpha^2 + \alpha_Z m_Z^2)\chi_3 \\
& - \bar{c}^+(\partial_\alpha^2 + \alpha_W m_W^2)c^- - \bar{c}^-(\partial_\alpha^2 + \alpha_Z m_W^2)c^+ \\
& - \bar{c}^Z(\partial_\alpha^2 + \alpha_Z m_Z^2)c^Z - \bar{c}^A\partial_\alpha^2 c^A
\end{aligned} \tag{B.61}$$

and define the interaction part by

$$\mathcal{L}_{int} = \mathcal{L} - \mathcal{L}_{tree}, \tag{B.62}$$

which contains all of the counterterms as well as tree interactions.

B.3 On-shell renormalization

The counterterms for all the physical particles introduced in Eqs. (B.44), (B.45), and (B.46) should be fixed by the renormalization conditions. They are the charge renormaliation and the on-shell conditions. The former is exactly the same as in QED. By "on-shell renormalization", I mean that,

1. the pole position of propagators should locate at physical mass,
2. residue of propagators at the pole should be unity.

The second condition allows one to omit any diagram whose external line contain self-energy insertion. This reduces the numbers of diagrams to be considered When one renormalizes gauge boson and fermion fields before symmetry breaking as discussed in the previous section, the resudes happen not to be unity, which means that the finite renormalition constants for wave

funtions of the external fields remains in the self-energy insertion diagrams. In the following, we do not expand the wave function renormalization constants to make the expressions compact. Writing them in a pertubation series, one can easily get the counterterms order by order.

B.3.1 Gauge boson renormalization

According to these requirements we can fix all counterterms for the propagators of physical particles. First, we consider the case of $W^{\pm}$ boson. We denote the contribution from irreducible self-energy diagram (vacuum polarization) as

$$\Pi^{W}_{\mu\nu}(q) = (g_{\mu\nu} - \frac{q_\mu q\nu}{q^2})a_W(q^2) + \frac{q_\mu q\nu}{q^2}b_W(q^2). \tag{B.63}$$

The corresponding counterterm, which is obtained from the Lagrangian by rescaling of the fields and mass counterterm, is given by

$$\begin{aligned}\Pi^{W}_{c\mu\nu}(q) &= (g_{\mu\nu} - \frac{q_\mu q\nu}{q^2})[\delta m^2_W \cdot Z_W - (q^2 - m^2_W)Z_W] \\ &+ \frac{q_\mu q\nu}{q^2}(\delta m^2_W \cdot Z_W + m^2_W Z_W).\end{aligned} \tag{B.64}$$

Adding these two and requiring that the ultraviolet divergence is cancelled, we define the renormalized self-energy functions of transverse and longitudinal parts,

$$\begin{aligned}\tilde{a}_W(q^2) &= a_W(q^2) + \delta m^2_W \cdot Z_W - (q^2 - m^2_W)Z_W, \\ \tilde{b}_W(q^2) &= b_W(q^2) + \delta m^2_W \cdot Z_W + m^2_W Z_W.\end{aligned} \tag{B.65}$$

The renormalization conditions are imposed on the transverse part of self-energy as

$$\tilde{a}_W(m^2_W) = 0, \qquad \tilde{a}^{'}_W(m^2_W) = 0, \tag{B.66}$$

where the prime means the derivative with respect to q^2. Hence we have, at one loop level,

$$\begin{aligned}\delta m^2_W &= -a(m^2_W), \\ Z_W &= a^{'}(m^2_W).\end{aligned} \tag{B.67}$$

Note that both δm^2_W and Z_W are fixed by these equations and the longitudinal part $b_W(q^2)$ is automatically made finite by these constants by virtue of the gauge invariance.

Next I discuss the neutral gauge boson sector and deal with the $\gamma - Z^0$ mixing term. The bare Lagrangian is diagonalized in terms of bare γ and Z^0 fields. Due to the renormalization procedure Eq... however, the renormalized γ and Z^0 fields make transition with each other, again. In other words we need the condition to determine Z_{AZ} and Z_{ZA} separately, while Z_{AA} and Z_{ZZ} are determined by the conditions (1) and (2). Let us consider the part of the Lagrangian which is bilinear in bare γ and Z^0 fields,

$$\mathcal{L}_{\gamma,Z_0} = -\frac{1}{4}Z_{\mu\nu 0}Z_{\mu\nu 0} - \frac{1}{2}m_{Z0}^2 Z_{\mu 0}Z_{\mu 0} - \frac{1}{4}F_{\mu\nu 0}F_{\mu\nu 0} + (\text{gauge fix.}), \quad \text{(B.68)}$$

where $Z_{\mu\nu 0}$ and $F_{\mu\nu 0}$ are field strengths defined by bare Z^0 and photon fields, $Z_{\mu 0}$ and $A_{\mu 0}$ like as $Z_{\mu\nu 0} = \partial_\mu Z_{\nu 0} - \partial_\nu Z_{\mu 0}$. Rewriting this by renormalization fields, we have

$$\begin{aligned}\mathcal{L}_{\gamma,Z_0} = \quad & -\frac{1}{4}[(Z_{ZZ}^{1/2})^2 + (Z_{AZ}^{1/2})^2]Z_{\mu\nu}Z_{\mu\nu} - \frac{1}{2}(m_Z^2 + \delta m_Z^2)(Z_{ZZ}^{1/2})^2 Z_\mu Z_\mu \\ & -\frac{1}{4}[(Z_{ZA}^{1/2})^2 + (Z_{AA}^{1/2})^2]F_{\mu\nu}F_{\mu\nu} - \frac{1}{2}(m_Z^2 + \delta m_Z^2)(Z_{ZA}^{1/2})^2 A_\mu A_\mu \\ & -\frac{1}{2}[Z_{ZA}^{1/2}Z_{ZZ}^{1/2} + Z_{AA}^{1/2}Z_{AZ}^{1/2}]F_{\mu\nu}F_{\mu\nu} - (m_Z^2 + \delta m_Z^2)Z_{ZA}^{1/2}Z_{ZZ}^{1/2}A_\mu Z_\mu. \end{aligned} \quad \text{(B.69)}$$

Thus the rescaling induces mixing among renormalized fields.

The contribution from a set of irreducible loop diagrams can be written in a form similar to for $W^\pm$. We denote them as follows:

$$\Pi_{\mu\nu}^Z(q) = (g_{\mu\nu} - \frac{q_\mu q\nu}{q^2})a_Z(q^2) + \frac{q_\mu q\nu}{q^2}b_Z(q^2) \quad \text{(B.70)}$$

for Z^0-Z^0 boson,

$$\Pi_{\mu\nu}^A(q) = (g_{\mu\nu} - \frac{q_\mu q\nu}{q^2})a_A(q^2) + \frac{q_\mu q\nu}{q^2}b_A(q^2) \quad \text{(B.71)}$$

for photon-photon and

$$\Pi_{\mu\nu}^{ZA}(q) = (g_{\mu\nu} - \frac{q_\mu q\nu}{q^2})a_{ZA}(q^2) + \frac{q_\mu q\nu}{q^2}b_{ZA}(q^2) \quad \text{(B.72)}$$

for photon-Z^0 mixing. The corresponding counterterms read from Eq.... are given by

$$
\begin{aligned}
\Pi^{Z}_{c\mu\nu}(q) &= (g_{\mu\nu} - \frac{q_\mu q\nu}{q^2})[(\delta m_{\rm Z}^2 + m_{\rm Z}^2)(Z_{ZZ}^{1/2})^2 - q^2((Z_{ZZ}^{1/2})^2 + (Z_{AZ}^{1/2})^2)] \\
&+ \frac{q_\mu q\nu}{q^2}(\delta m_{\rm Z}^2 + m_{\rm Z}^2)(Z_{ZZ}^{1/2})^2, \\
\Pi^{A}_{c\mu\nu}(q) &= (g_{\mu\nu} - \frac{q_\mu q\nu}{q^2})[(\delta m_{\rm Z}^2 + m_{\rm Z}^2)(Z_{ZA}^{1/2})^2 - q^2((Z_{ZA}^{1/2})^2 + (Z_{AA}^{1/2})^2)] \\
&+ \frac{q_\mu q\nu}{q^2}(\delta m_{\rm Z}^2 + m_{\rm Z}^2)(Z_{ZA}^{1/2})^2, \\
\Pi^{Z}A_{c\mu\nu}(q) &= (g_{\mu\nu} - \frac{q_\mu q\nu}{q^2})[(\delta m_{\rm Z}^2 + m_{\rm Z}^2)Z_{ZZ}^{1/2}Z_{ZA}^{1/2} - q^2(Z_{ZZ}^{1/2}Z_{ZA}^{1/2} + Z_{AA}^{1/2}Z_{ZA}^{1/2})] \\
&+ \frac{q_\mu q\nu}{q^2}(\delta m_{\rm Z}^2 + m_{\rm Z}^2)Z_{ZZ}^{1/2}Z_{ZA}^{1/2}. \qquad \text{(B.73)}
\end{aligned}
$$

In order to make the renormalized self-energies finite, which are defined by

$$
\begin{aligned}
\tilde{a}_Z(q^2) &= a_Z(q^2) + (\delta m_{\rm Z}^2 + m_{\rm Z}^2)(Z_{ZZ}^{1/2})^2 - q^2((Z_{ZZ}^{1/2})^2 + (Z_{AZ}^{1/2})^2), \\
\tilde{a}_Z(q^2) &= a_A(q^2) + (\delta m_{\rm Z}^2 + m_{\rm Z}^2)(Z_{ZA}^{1/2})^2 - q^2((Z_{ZA}^{1/2})^2 + (Z_{AA}^{1/2})^2), \\
\tilde{a}_{ZA}(q^2) &= a_{ZA}(q^2) + (\delta m_{\rm Z}^2 + m_{\rm Z}^2)Z_{ZZ}^{1/2}Z_{ZA}^{1/2} - q^2(Z_{ZZ}^{1/2}Z_{ZA}^{1/2} + Z_{AA}^{1/2}Z_{ZA}^{1/2}),
\end{aligned} \qquad \text{(B.74)}
$$

we require the following renormalization conditions:

$$
\begin{aligned}
\tilde{a}_Z(m_{\rm Z}^2) &= 0, \quad & \tilde{a}_Z^{'}(m_{\rm Z}^2) &= 0, \\
\tilde{a}_Z(0) &= 0, \quad & \tilde{a}_Z^{'}(0) &= 0, \\
\tilde{a}_{ZA}(m_{\rm Z}^2) &= 0, \quad & \tilde{a}_{ZA}^{'}(0) &= 0.
\end{aligned}
$$

It should be noted that two conditions $\tilde{a}_Z(0)$ and $\tilde{a}_{ZA}^{'}(0) = 0$ are identical due to the Ward-Takahashi identity for the electromagnatic interation. The later condition has the meaning that the γ-Z^0 mixing diagram should not develope a pole at $q^2 = 0$. Thus we have five conditions by which four Z's and one $m_{\rm Z}^2$ are determined. The longitudinal parts $b_Z(q^2)$, $b_A(q^2)$ and $b_{ZA}(q^2)$ are again renormalized by these constants. A comment is in order; including the lowest order corrections, two constants, $Z_{ZZ}^{1/2}$ and $Z_{AA}^{1/2}$, are the quantities of $1 + \mathcal{O}(\alpha)$, while the other two, $Z_{ZA}^{1/2}$ and $Z_{AZ}^{1/2}$, are $\mathcal{O}(\alpha)$ by themselves. General solutions for the Z's are very complicated, but in the one-loop order we can express them by self-energies in the following simple forms:

$$
\begin{aligned}
\delta m_{\rm Z}^2 &= -a_Z(m_{\rm Z}^2), \\
2Z_{ZZ}^{1/2} &= a_Z^{'}(m_{\rm Z}^2), \\
2Z_{AA}^{1/2} &= a_Z^{'}(0), \\
Z_{ZA}^{1/2} &= -a_{ZA}^{'}(0)/m_{\rm Z}^2, \\
Z_{AZ}^{1/2} &= a_{ZA}^{'}(m_{\rm Z}^2)/m_{\rm Z}^2.
\end{aligned} \qquad \text{(B.75)}
$$

B.3.2 Higgs scalar renormalization

The renormalization of Higgs field can be done in the same way as other physical particles. The counterterm is given by

$$\Sigma_{\phi C}(q^2) = -\delta m_H^2 Z_\phi + (q^2 - m_H^2) Z_\phi + 3T_0 Y \frac{eM_Z}{2m_W\sqrt{m_Z^2 - m_W^2}} G_3 H^{-1} Z_\phi, \tag{B.76}$$

which defines the renormalized self-energy by

$$\tilde{\Sigma}_{\phi C}(q^2) = \Sigma_{\phi C}(q^2) + \Sigma_\phi(q^2) \tag{B.77}$$

which the on-shell conditions,

$$\begin{aligned} \tilde{\Sigma}_\phi(m_H^2) &= 0, \\ \tilde{\Sigma_\phi'}(m_H^2) &= 0, \end{aligned} \tag{B.78}$$

which determines both Z_ϕ and δm_H^2.

I do not show the explicit procedure to renormalize Goldstone bosons and ghost particles, because they are not necessary for the subjects discussed in this article. It is performed in a way similar to the above prescription. Interested readers can find its details in [13]. It is sufficient to point out here that these unphysical particles never appear in the external lines and only contribute to the loop diagrams.

Bibliography

[1] E. Ward, Estimated matter-energy content of the universe, http://cds.cern.ch/record/2665176.

[2] The International Linear Collider Technical Design Report - Volume 1: Executive SummaryarXiv:1306.6327.

[3] M. E. P. Keisuke Fujii, Christophe Grojean, Physics case for the 250 gev stage of the international linear colliderarXiv:1710.07621v4.

[4] Planck reveals an almost perfect universe, http://www.esa.int/Science_Exploration/Space_Science/Planck/Planck_reveals_an_almost_perfect_Universe.

[5] G. Aad, et al., Observation of a new particle in the search for the Standard Model Higgs boson with the ATLAS detector at the LHC, Phys. Lett. B 716 (2012) 1–29. arXiv:1207.7214, doi:10.1016/j.physletb.2012.08.020.

[6] S. Chatrchyan, et al., Observation of a New Boson at a Mass of 125 GeV with the CMS Experiment at the LHC, Phys. Lett. B 716 (2012) 30–61. arXiv:1207.7235, doi:10.1016/j.physletb.2012.08.021.

[7] K. Fujii, Physics at the ILC with focus mostly on Higgs physics, in: 1st Toyama International Workshop on Higgs as a Probe of New Physics 2013, 2013. arXiv:1305.1692.

[8] N. M. U. Quach, Y. Kurihara, K. H. Phan, T. Ueda, Beam polarization effects on top-pair production at the ILC, Eur. Phys. J. C 78 (5) (2018) 422. arXiv:1706.03432, doi:10.1140/epjc/s10052-018-5895-9.

[9] G. Belanger, F. Boudjema, J. Fujimoto, T. Ishikawa, T. Kaneko, K. Kato, Y. Shimizu, Automatic calculations in high energy physics and Grace at one-loop, Phys. Rept. 430 (2006) 117–209. arXiv:hep-ph/0308080, doi:10.1016/j.physrep.2006.02.001.

[10] Grace home page, https://minami-home.kek.jp/.

[11] J. Fujimoto, T. Ishikawa, M. Jimbo, T. Kon, Y. Kurihara, M. Kuroda, Two-body and Three-body Decays of Charginos in One-loop Order in MSSMarXiv:hep-ph/0701200.

[12] J. A. M. Vermaseren, New features of FORMarXiv:0010025.

[13] K.-i. Aoki, Z. Hioki, R. Kawabe, M. Konuma, T. Muta, Electroweak Theory: Framework of On-Shell Renormalization and Study of Higher-Order Effects, Progress of Theoretical Physics Supplement 73 (1982) 1–226. arXiv:https://academic.oup.com/ptps/article-pdf/doi/10.1143/PTPS.73.1/5229023/73-1.pdf, doi:10.1143/PTPS.73.1.
URL https://doi.org/10.1143/PTPS.73.1

[14] F. Boudjema, E. Chopin, Double Higgs production at the linear colliders and the probing of the Higgs selfcoupling, Z. Phys. C 73 (1996) 85–110. arXiv:hep-ph/9507396, doi:10.1007/s002880050298.

[15] M. Tanabashi, K. Hagiwara, K. Hikasa, K. Nakamura, Y. Sumino, F. Takahashi, J. Tanaka, K. Agashe, G. Aielli, C. Amsler, M. Antonelli, D. M. Asner, H. Baer, S. Banerjee, R. M. Barnett, T. Basaglia, C. W. Bauer, J. J. Beatty, V. I. Belousov, J. Beringer, S. Bethke, A. Bettini, H. Bichsel, O. Biebel, K. M. Black, E. Blucher, O. Buchmuller, V. Burkert, M. A. Bychkov, R. N. Cahn, M. Carena, A. Ceccucci, A. Cerri, D. Chakraborty, M.-C. Chen, R. S. Chivukula, G. Cowan, O. Dahl, G. D'Ambrosio, T. Damour, D. de Florian, A. de Gouvêa, T. DeGrand, P. de Jong, G. Dissertori, B. A. Dobrescu, M. D'Onofrio, M. Doser, M. Drees, H. K. Dreiner, D. A. Dwyer, P. Eerola, S. Eidelman, J. Ellis, J. Erler, V. V. Ezhela, W. Fetscher, B. D. Fields, R. Firestone, B. Foster, A. Freitas, H. Gallagher, L. Garren, H.-J. Gerber, G. Gerbier, T. Gershon, Y. Gershtein, T. Gherghetta, A. A. Godizov, M. Goodman, C. Grab, A. V. Gritsan, C. Grojean, D. E. Groom, M. Grünewald, A. Gurtu, T. Gutsche, H. E. Haber, C. Hanhart, S. Hashimoto, Y. Hayato, K. G. Hayes, A. Hebecker, S. Heinemeyer, B. Heltsley, J. J. Hernández-Rey, J. Hisano, A. Höcker, J. Holder, A. Holtkamp, T. Hyodo, K. D. Irwin, K. F. Johnson, M. Kado, M. Karliner, U. F. Katz, S. R. Klein, E. Klempt, R. V. Kowalewski, F. Krauss, M. Kreps, B. Krusche, Y. V. Kuyanov, Y. Kwon, O. Lahav, J. Laiho, J. Lesgourgues, A. Liddle, Z. Ligeti, C.-J. Lin, C. Lippmann, T. M. Liss, L. Littenberg, K. S. Lugovsky, S. B. Lugovsky, A. Lusiani, Y. Makida, F. Maltoni, T. Mannel, A. V. Manohar, W. J. Marciano, A. D. Martin, A. Masoni, J. Matthews, U.-G. Meißner, D. Milstead, R. E. Mitchell, K. Mönig, P. Molaro, F. Moortgat, M. Moskovic, H. Murayama, M. Narain, P. Nason, S. Navas, M. Neubert, P. Nevski, Y. Nir, K. A. Olive, S. Pagan Griso, J. Parsons, C. Patrignani, J. A. Peacock, M. Pennington, S. T. Petcov, V. A. Petrov, E. Pianori, A. Piepke, A. Pomarol, A. Quadt, J. Rademacker, G. Raffelt, B. N. Ratcliff, P. Richardson, A. Ringwald, S. Roesler, S. Rolli, A. Romaniouk, L. J. Rosenberg, J. L. Rosner, G. Rybka, R. A. Ryutin, C. T. Sachrajda, Y. Sakai, G. P. Salam, S. Sarkar, F. Sauli, O. Schneider, K. Scholberg, A. J. Schwartz, D. Scott, V. Sharma, S. R. Sharpe, T. Shutt, M. Silari, T. Sjöstrand, P. Skands, T. Skwarnicki, J. G. Smith, G. F. Smoot, S. Spanier, H. Spieler, C. Spiering, A. Stahl, S. L. Stone, T. Sumiyoshi, M. J. Syphers, K. Terashi, J. Terning, U. Thoma, R. S. Thorne, L. Tiator, M. Titov, N. P. Tkachenko, N. A. Törnqvist, D. R. Tovey, G. Valencia, R. Van de Water, N. Varelas, G. Venanzoni, L. Verde,

M. G. Vincter, P. Vogel, A. Vogt, S. P. Wakely, W. Walkowiak, C. W. Walter, D. Wands, D. R. Ward, M. O. Wascko, G. Weiglein, D. H. Weinberg, E. J. Weinberg, M. White, L. R. Wiencke, S. Willocq, C. G. Wohl, J. Womersley, C. L. Woody, R. L. Workman, W.-M. Yao, G. P. Zeller, O. V. Zenin, R.-Y. Zhu, S.-L. Zhu, F. Zimmermann, P. A. Zyla, J. Anderson, L. Fuller, V. S. Lugovsky, P. Schaffner, Review of particle physics, Phys. Rev. D 98 (2018) 030001. doi:10.1103/PhysRevD.98.030001.
URL https://link.aps.org/doi/10.1103/PhysRevD.98.030001

[16] Z. Hioki, How Does the Discovery of Z Boson Improve the Prediction for $W^{\pm}$ Boson Mass?, Progress of Theoretical Physics 68 (6) (1982) 2134–2140. arXiv:https://academic.oup.com/ptp/article-pdf/68/6/2134/5312239/68-6-2134.pdf, doi:10.1143/PTP.68.2134.
URL https://doi.org/10.1143/PTP.68.2134

[17] J. Fujimoto, Y. Kurihara, N. M. Quach, $\mathcal{O}(\alpha^2)$ ISR effects with a full electroweak one-loop correction for a top pair-production at the ILC, Eur. Phys. J. C 79 (6) (2019) 506. arXiv:1802.07826, doi:10.1140/epjc/s10052-019-7026-7.

[18] S. Kawabata, A new version of the multi-dimensional integration and event generation package bases/spring, Computer Physics Communications 88 (2) (1995) 309 – 326. doi:https://doi.org/10.1016/0010-4655(95)00028-E.
URL http://www.sciencedirect.com/science/article/pii/001046559500028E

[19] H. K. Phan, Full one-loop electroweak radiativecorrections at future colliders, Ph.D. thesis, The Graduate University for Advanced Studies (2014).

[20] A. Denner, S. Dittmaier, M. Roth, M. Weber, Electroweak radiative corrections to e+ e- —> nu anti-nu H, Nucl. Phys. B 660 (2003) 289–321. arXiv:hep-ph/0302198, doi:10.1016/S0550-3213(03)00269-4.

[21] T. Lee, M. Nauenberg, Degenerate Systems and Mass Singularities, Phys. Rev. 133 (1964) B1549–B1562. doi:10.1103/PhysRev.133.B1549.

[22] T. Kinoshita, Mass singularities of Feynman amplitudes, J. Math. Phys. 3 (1962) 650–677. doi:10.1063/1.1724268.